An ependymal cell atlas reveals heterogeneous ongoing cell maturation in the adult mouse spinal cord that is dynamically regulated by injury

Resource

Developmental Cell

An ependymal cell census identifies heterogeneous and ongoing cell maturation in the adult mouse spinal cord that changes dynamically on injury

Graphical abstract

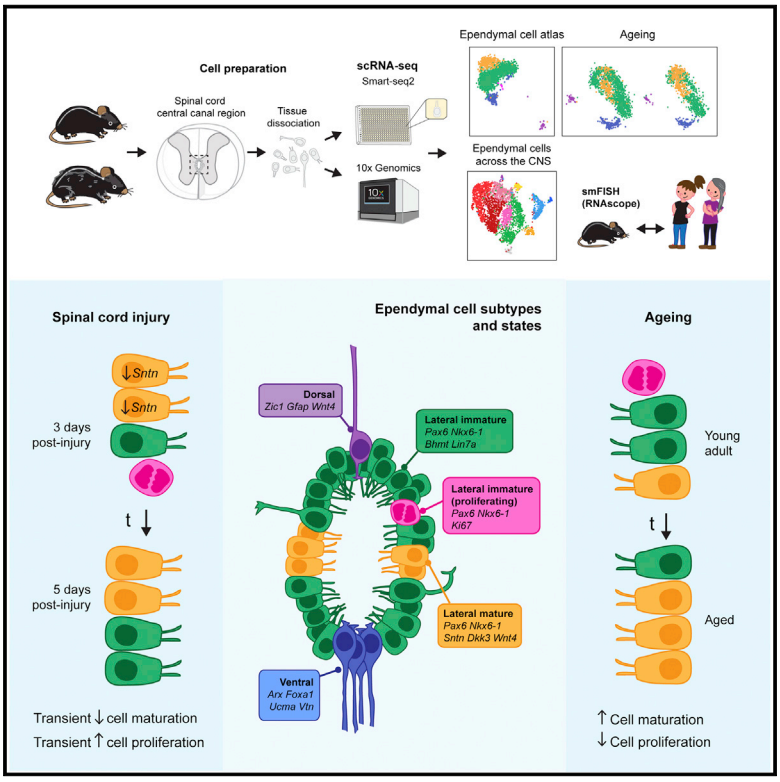

Highlights

- Single-cell transcriptomic profiling of adult mouse spinal cord ependymal cells
- Identification of immature ependymal cells as potential spinal cord stem cells
- Spinal cord injury induces transient reversal of cell maturation
- Ependymal cell identities in the adult spinal cord differ between mice and humans

Authors

Aida Rodrigo Albors, Gail A. Singer, Enric Llorens-Bobadilla, Jonas Frisén, Andrew P. May, Chris P. Ponting, Kate G. Storey

Correspondence

a.rodrigoalbors@dundee.ac.uk (A.R.A.), k.g.storey@dundee.ac.uk (K.G.S.)

In brief

Rodrigo Albors et al. profile the heterogeneous population of ependymal cells in the adult mouse spinal cord. Computationally and using spinal cord injury assays, they identify immature cells as potential spinal cord stem cells and uncover widespread cell maturation and altered cell identities in the human adult spinal cord.

Rodrigo Albors et al., 2023, Developmental Cell *58*, 1–17
February 6, 2023
https://doi.org/10.1016/j.devcel.2023.01.003

CellPress

Developmental Cell

CellPress
OPEN ACCESS

Resource

An ependymal cell census identifies heterogeneous and ongoing cell maturation in the adult mouse spinal cord that changes dynamically on injury

Aida Rodrigo Albors,[1,*] Gail A. Singer,[1] Enric Llorens-Bobadilla,[2] Jonas Frisén,[2] Andrew P. May,[3,4] Chris P. Ponting,[5] and Kate G. Storey[1,6,*]

[1]Division of Molecular, Cell and Developmental Biology, School of Life Sciences, University of Dundee, Dundee DD1 5EH, UK
[2]Department of Cell and Molecular Biology, Karolinska Institutet, 171 77 Stockholm, Sweden
[3]Chan Zuckerberg Biohub, San Francisco, CA 94158, USA
[4]Tornado Bio, Inc., South San Francisco, CA 94080, USA
[5]Medical Research Council Human Genetics Unit, Institute of Genetics and Cancer, University of Edinburgh, Edinburgh EH4 2XU, UK
[6]Lead contact
*Correspondence: a.rodrigoalbors@dundee.ac.uk (A.R.A.), k.g.storey@dundee.ac.uk (K.G.S.)
https://doi.org/10.1016/j.devcel.2023.01.003

SUMMARY

The adult spinal cord stem cell potential resides within the ependymal cell population and declines with age. Ependymal cells are, however, heterogeneous, and the biological diversity this represents and how it changes with age remain unknown. Here, we present a single-cell transcriptomic census of spinal cord ependymal cells from adult and aged mice, identifying not only all known ependymal cell subtypes but also immature as well as mature cell states. By comparing transcriptomes of spinal cord and brain ependymal cells, which lack stem cell abilities, we identify immature cells as potential spinal cord stem cells. Following spinal cord injury, these cells re-enter the cell cycle, which is accompanied by a short-lived reversal of ependymal cell maturation. We further analyze ependymal cells in the human spinal cord and identify widespread cell maturation and altered cell identities. This in-depth characterization of spinal cord ependymal cells provides insight into their biology and informs strategies for spinal cord repair.

INTRODUCTION

Ependymal cells are ciliated cells lining the brain ventricles and the spinal cord central canal and key components of the ventricular-subventricular zone and central canal stem cell niches.[1–4] Although it is well established in the adult mouse brain that ependymal cells are postmitotic and the neural stem cell potential resides within subependymal adult neural stem cells,[5–10] some spinal cord ependymal cells can behave as neural stem cells. From axolotls and zebrafish to mice, spinal cord ependymal cells can self-renew and generate specialized cells after injury and *in vitro*.[11–24] However, the ability to repair the spinal cord varies greatly between species and spinal cord injuries continue to lead to permanent disability in mice and humans.[3,25,26] In mice, ependymal cells generate mostly scar-forming astrocytes and a few oligodendrocytes following spinal cord injury. Although ependymal-derived astrocytes are essential to prevent further damage,[27] oligodendrocytes are not replaced in sufficient numbers, new neurons are not generated, and function is not restored.[11,12,28] Ependymal cells in the human spinal cord have not been observed proliferating[14,29,30] but do display neural stem cell characteristics when cultured *in vitro*.[14,18,31] Much research has been focused on harnessing this endogenous cell population to enhance spinal cord repair.[32] However, ependymal cells in mice and humans are highly heterogeneous, and we know surprisingly little about what this heterogeneity represents.

Morphologically, mouse spinal cord ependymal cells are usually classified into radial, cuboidal, and tanycytes.[11,33,34] Based on a handful of molecular markers, ependymal cells are also molecularly heterogeneous.[11,33,35–37] Single-cell RNA sequencing (scRNA-seq) technologies now make it possible to profile ependymal cells in an unbiased way, with the necessary cellular resolution. However, ependymal cells represent a very small fraction of the cells that make up the adult spinal cord and are difficult to dissociate into single cells. Consequently, ependymal cells are underrepresented in broader single-cell atlases of the spinal cord.[38,39] A few single-cell studies have focused on a subset of spinal cord ependymal cells but did not delve into their heterogeneity.[20,21,40] Although the neural stem cell potential of some ependymal cell subtypes has been demonstrated,[21,35,41] whether mouse ependymal cell diversity reflects different functions and regenerative capabilities remains unknown. Human spinal cord ependymal cells appear similarly heterogeneous and undergo dramatic changes with age. In infants and teenagers, ependymal cells resemble those of adult mice and organize around the central canal, but in adults, this

Please cite this article in press as: Rodrigo Albors et al., An ependymal cell census identifies heterogeneous and ongoing cell maturation in the adult mouse spinal cord that changes dynamically on injury, Developmental Cell (2023), https://doi.org/10.1016/j.devcel.2023.01.003

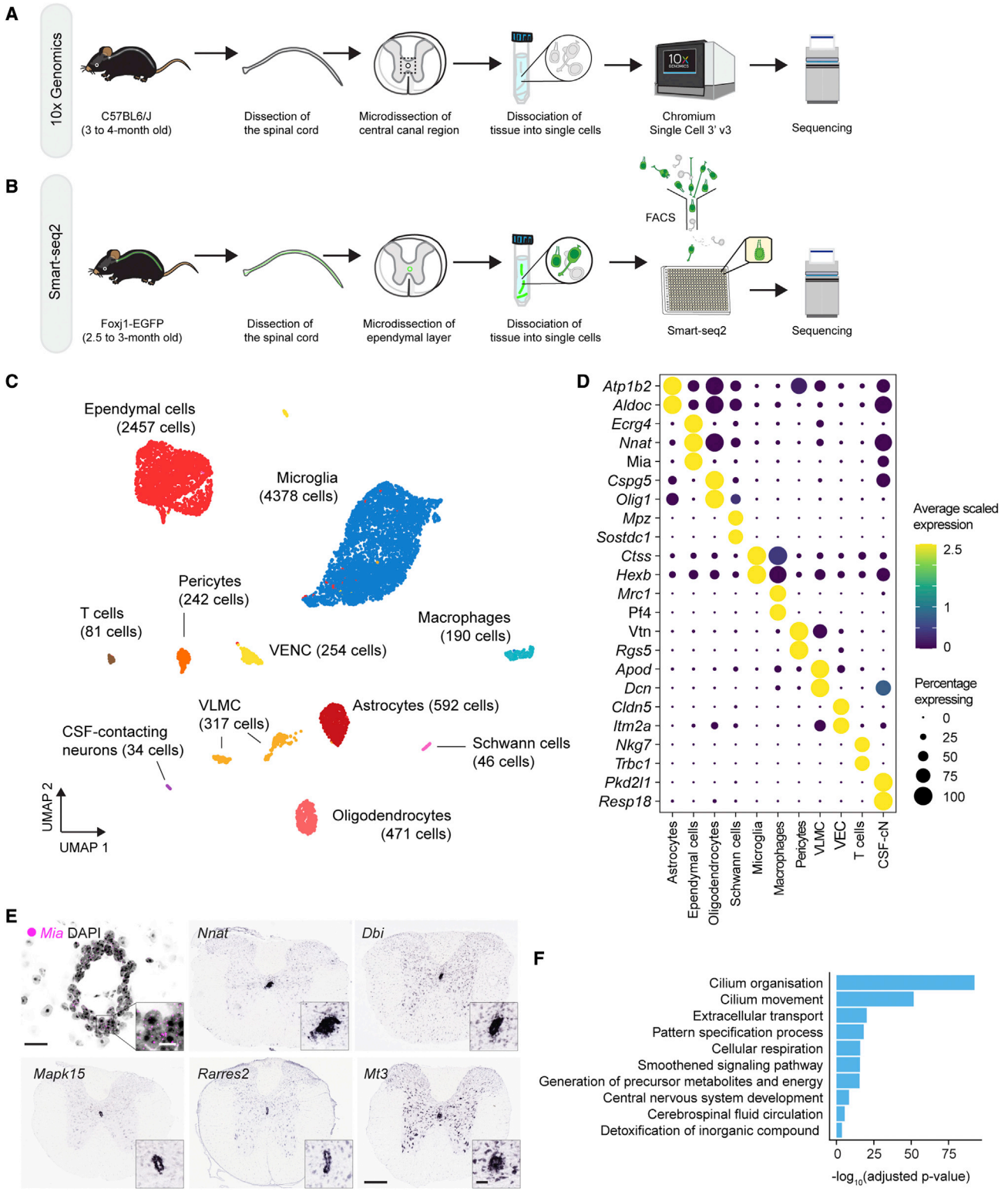

Figure 1. A cell map of the spinal cord central canal region

(A and B) (A) Workflow for the generation of 10x and (B) Smart-seq2 scRNA-seq datasets.

(C) UMAP embedding of cells from the central canal region.

(D) Average expression of selected marker genes for each cell type in (C), and percentage of cells within each cluster expressing each gene.

(legend continued on next page)

structure tends to collapse into an ependymal cell mass.[29,36,42–45] How human and mouse ependymal cells align and what molecular changes ependymal cells undergo with age are poorly understood.

Here, we generate a single-cell transcriptomic census of spinal cord ependymal cells in mice, identifying genes for all known subtypes and immature and mature cell states. We discover a delay in the maturation of lateral ependymal cells that distinguishes these cells from their non-regenerative brain counterparts. Following spinal cord injury, we show that ependymal cell maturation is dynamically lost but rapidly regained, underscoring the limited regenerative potential of mature cells. Informed by our mouse data, we provide evidence for early ependymal cell maturation in the human spinal cord and surprising age-related changes in ependymal cell identity.

RESULTS

A cell map of the spinal cord central canal region

To characterize spinal cord ependymal cells comprehensively, we took two complementary scRNA-seq approaches: droplet-based 3′ scRNA-seq (10x Genomics), to profile a large number of cells in and around the central canal, and plate-based full-length scRNA-seq (Smart-seq2), to profile ependymal cells in depth. Using the 10x approach, we profiled cells from young adult (3–4 months old) wild-type mice (Figures 1A and S1). For the Smart-seq2 dataset, we isolated GFP-positive ependymal cells from age-matched (2.5–3 months old) FOXJ1-EGFP reporter mice[46] (Figure 1B). We first focused on the broader 10x dataset to explore the unique features of ependymal cells compared with other cells in the central canal region. The cells partitioned into 27 clusters (Figure S1B), which we annotated into 11 cell types based on the expression of known marker genes (Figures 1C and 1D; Table S1). Microglia was the most abundant cell type represented in the dataset, followed by ependymal cells, oligodendrocyte-lineage cells, astrocytes, vascular leptomeningeal cells, vascular endothelial cells, pericytes, macrophages, T cells, and cerebrospinal fluid (CSF)-contacting neurons.

Differential expression analysis identified *Ecrg4* and *Mia* as two genes whose expression is most enriched in ependymal cells (Figure 1D; Table S1). Using RNAscope, we confirmed that *Mia* is highly expressed in ependymal cells (Figure 1E). We also established that the expression of some ependymal-enriched genes is consistent with *in situ* hybridization data from the Allen Brain Atlas (http://mousespinal.brain-map.org/) (Figure 1E). To infer the biological functions of ependymal cells, we performed a gene ontology (GO) enrichment analysis on the full list of ependymal-enriched genes (Figure 1F). Genes associated with cilium-related terms were overrepresented, consistent with the role of ependymal cilia contributing to CSF flow.[33,47,48] GO terms extracellular transport and detoxification of inorganic compounds were also overrepresented, highlighting ependymal regulation of CSF composition (Table S1).

Ependymal cells in the mouse spinal cord are transcriptionally heterogeneous

Ependymal cells derive from three embryonic progenitor domains: the roof plate,[49,50] floor plate,[36,51,52] and p2 and motor neuron progenitors (pMN) domains.[36,53–55] However, little is known about the molecular makeup and functions of these ependymal subtypes. To explore ependymal cell heterogeneity in detail, we subset the ependymal cell cluster from the 10x dataset and integrated it with the Smart-seq2 dataset (Figures S2A and S2B). Clustering revealed six ependymal cell subtypes and states (Figures 2A and S2C). Consistent with their developmental origins, all ependymal cells expressed one of the three sets of domain-specific genes. Dorsal ependymal cells expressed the roof plate marker *Zic1*,[56] ventral ependymal cells expressed the floor plate marker *Arx*,[57] and all other ependymal cell clusters co-expressed *Pax6* and *Nkx6-1*, characteristic of embryonic p2 and pMN progenitors (Figure 2C). Due to the location of the latter within the central canal,[36,53] we refer to these cells as lateral ependymal cells.

To identify genes further defining ependymal cell subtypes and infer their functions, we performed differential expression and GO analyses (Tables S2 and S3). Dorsal ependymal cells expressed Zic transcription factors (*Zic1*, *Zic2*, *Zic4*, and *Zic5*) and the highest levels of intermediate filament genes *Gfap* and nestin (*Nes*) (Figures 2C and 2D). These cells also expressed genes encoding signaling molecules (e.g., *Bmp6* and *Wnt4*) (Figures 2C–2E). Using RNAscope, we confirmed that a small subset of dorsally located ependymal cells co-expressed *Zic1* and *Wnt4* (Figures 2D, 2E, and S3A). Biological processes associated with dorsal cells included nervous system development, cell differentiation, regulation of growth, regulation of signaling, and regulation of synaptic plasticity (Figure 2F). Indeed, cellular component terms associated with dorsal cells (e.g., synapse) suggest that these cells may interact with neurons. These findings imply that dorsal ependymal cells retain some functions of embryonic radial glial cells including providing structural support and contributing to the signaling microenvironment in the central canal niche.

In addition to *Arx* (Figure 2C),[36,52] ventral ependymal cells expressed other floor plate genes such as *Ntn1*,[58] *Sulf1*, secreted bone morphogenetic protein (BMP) inhibitors *Nbl1* and *Ucma*,[59,60] and the cell adhesion and spreading factor *Vtn* (Figures 2C and 2D). We confirmed that *Vtn* and *Ucma* are co-expressed by ventrally located ependymal cells, around 10% of the ependymal cell population (Figures 2D, 2E, and S3B). GO analysis revealed glycosaminoglycan binding, growth factor binding, and metal chelating activity among molecular functions associated with ventral cells, and biological processes included the regulation of cell migration, the negative regulation of signal transduction, and G_1 to G_0 transition (Figure 2E; Table S3). From these findings, we infer that ventral ependymal cells are quiescent or postmitotic cells and major contributors of cell-extrinsic factors to the niche.

Lateral ependymal cells partitioned into four cell states (Figure 2A). An intriguing subset was enriched in cilia-related genes

(E) Close up of the central canal region showing RNAscope for *Mia* and *in situ* hybridization images from the Allen Brain Atlas showing the expression of ependymal-enriched genes. Scale bars: 30 and 10 μm (insets) (RNAscope) and 200 and 50 μm (Allen Brain Atlas).
(F) Selected GO terms associated with genes whose expression is enriched in ependymal cells. Bars show biological processes significantly overrepresented ranked by adjusted p value (false discovery rate [FDR]).

Please cite this article in press as: Rodrigo Albors et al., An ependymal cell census identifies heterogeneous and ongoing cell maturation in the adult mouse spinal cord that changes dynamically on injury, Developmental Cell (2023), https://doi.org/10.1016/j.devcel.2023.01.003

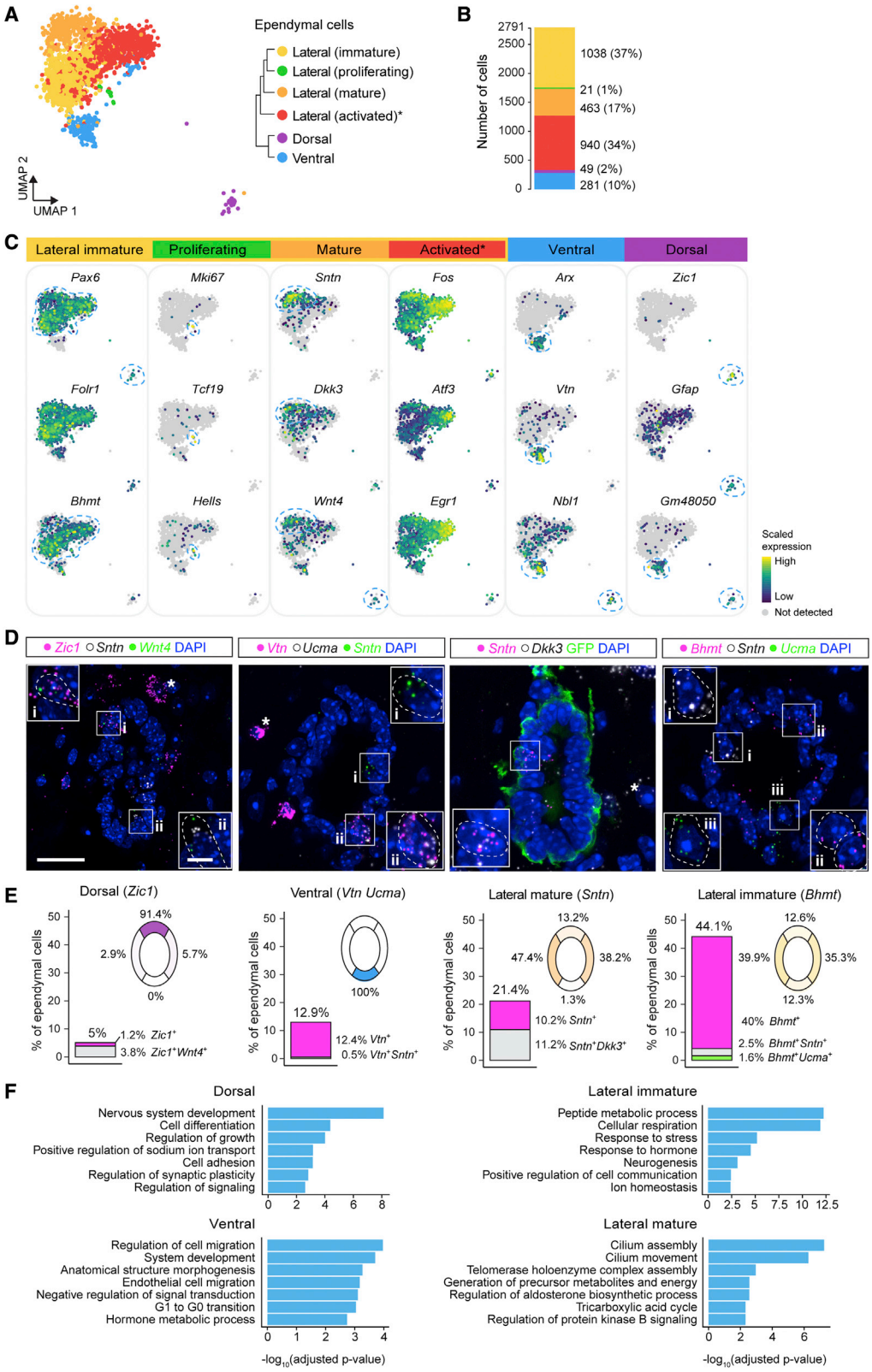

Figure 2. A cell map of spinal cord ependymal cells

(A) UMAP embedding of spinal cord ependymal cell transcriptomes captured using 10x and Smart-seq2 scRNA-seq technologies. Dendrogram shows the relationship between ependymal cell subtypes and states.

(legend continued on next page)

Please cite this article in press as: Rodrigo Albors et al., An ependymal cell census identifies heterogeneous and ongoing cell maturation in the adult mouse spinal cord that changes dynamically on injury, Developmental Cell (2023), https://doi.org/10.1016/j.devcel.2023.01.003

and uniquely expressed *Sntn*, a FOXJ1 effector that encodes for the apical ciliary protein Sentan[61,62] (Figures 2C–2E). *Sntn* expression reflects the structural and functional maturation of postnatal ciliated airway cells[62,63] and is commonly used as a marker of mature cells in multiciliated epithelia,[61,63–65] suggesting that it marks mature ependymal cells. Consistent with this, other molecular features of *Sntn* cells such as higher expression of the cyclin-dependent kinase inhibitor p21 gene (*Cdkn1a*) and histone genes (*Hist1h1c*, *Hist1h4h*, and *Hist1h4i*) suggest the acquisition of a postmitotic state and distinct chromatin organization. *Sntn* cells also expressed *Phlda3*, a p53-regulated repressor of Akt and potential tumor suppressor.[66,67] Importantly, *Sntn* cells expressed the highest levels of *Dkk3*, a negative regulator of Wnt signaling,[68] and *Wnt4* (Figures 2C and 2D), a ligand involved in non-canonical Wnt signaling that induces quiescence in other stem cell niches.[69,70] We confirmed that ~21% of ependymal cells express *Sntn* and many of these cells co-express *Dkk3* and *Wnt4* in the lateral walls of the central canal (Figures 2D, 2E, and S3C). Biological processes overrepresented in *Sntn* cells included tricarboxylic acid cycle and aerobic respiration (Figure 2G). By contrast, genes more highly expressed in *Sntn*-negative lateral cells included ribosomal genes, characteristic of more active cells[71,72] (Table S2). Indeed, a small fraction of captured *Sntn*-negative lateral cells were proliferating, inferred by the expression of cell cycle genes (e.g., *Mki67*) (Figure 2C). *Sntn*-negative lateral cells were also characterized by the expression of *Bhmt* (Figures 2C and 2D), encoding an enzyme involved in the BHMT-betaine pathway. We found that *Bhmt* is uniquely expressed by ependymal cells and confirmed that *Bhmt*-positive *Sntn*-negative cells make up most cells in the lateral walls of the central canal (Figures 2E and S3D). These distinct gene expression profiles within the lateral ependymal cell subpopulation suggest that these cells co-exist as mature and immature cells in the adult mouse spinal cord.

A subset of immature *Sntn*-negative lateral cells was also characterized by high levels of immediate early genes (including *Fos*, *Junb*, and *Egr1*) and other known stress-induced genes (e.g., *Maff* and *Ccn1*) (Figure 2C; Table S2). Ependymal cells with a similar gene expression signature are also evident in other scRNA-seq studies.[38,40] To assess whether such an "activated" ependymal cell subset exists *in vivo*, we performed RNAscope for *Fos* in the intact spinal cord and found that only a small fraction of ependymal cells express *Fos* (Figures S4A and S4B). This indicates that this ependymal cell subset likely reflects experimental manipulation and does not exist *in vivo*. However, despite the presence of such cells, our spinal cord ependymal cell census captures the transcriptomes of all known ependymal cell subtypes and uncovers immature and mature cell states of lateral ependymal cells.

The fraction of mature spinal cord ependymal cells increases with age

The ability of ependymal cells to proliferate and function as neural stem cells declines over time,[33,73] and this prompted us to investigate how ependymal cells change with age. To do so while minimizing technical variability between samples, we generated a 10x scRNA-seq dataset from cells in and around the central canal region of aged mice (18–19 months) in parallel with the young adult dataset (3–4 months) (Figures 1 and 3A). We recovered the same major cell types from the aged and from the young central canal (Figure 3B) but observed age-related heterogeneity (Figures S5A–S5C).

We focused on age-related changes in ependymal cells. Clustering revealed that ependymal cell identity was largely maintained in the aged spinal cord (Figure 3C). Indeed, we identified the same ependymal cell subtypes and states in young and aged mice except for the proliferating cell cluster, consistent with the decrease in ependymal cell proliferation with age.[33,35] To uncover potential age-related expression changes, we performed differential gene expression analysis between young and aged cells and found that ependymal cell transcriptomes from young and aged mice were surprisingly similar. We only detected 54 age-regulated genes in cells from aged mice, 34 upregulated and 20 downregulated (Table S4). Genes upregulated in aged ependymal cells were associated with mitochondrial function (e.g., *mt-Atp6* and *mt-Cytb*), glutathione metabolism (*Gstm1*, *Gpx3*, and *Mgst1*), and immune-related processes (e.g., *Lyz2* and *Mif*). Genes downregulated in aged cells included *Mt3*, a metallothionein protein involved in protecting against heavy metal toxicity; *Pcsk2*, a protease involved in processing protein precursors; and the cell cycle gene *Ccnd2*.

Analysis of the relative abundance of ependymal cell subtypes in young and aged mice revealed that lateral ependymal cells shift toward a mature cell state. Immature lateral cells decreased from 56% in young mice to 43% in aged mice (from 71% to 47% if also considering immature lateral cells expressing high levels of immediate early genes), whereas the percentage of mature cells increased from 17% to 40% (Figure 3D). By contrast, the percentage of dorsal and ventral ependymal cells did not change postnatally (Figure 3D). To confirm and extend these observations, we investigated the expression of subtype-specific markers across a wider range of ages using RNAscope (Figure 3E). Ependymal cells first appear in the developing mouse spinal cord between embryonic day (E) 15.5 and E17.5, and by E18.5, the ventricular layer of the developing spinal cord reaches the size of the future central canal.[19,52] At E18.5, just ~3% ependymal cells expressed *Sntn* (Figures 3E and 3F). The percentage of *Sntn*-expressing cells increased postnatally with 15% of ependymal cells expressing *Sntn* at postnatal day (P) 21, 19% in 3-month-old mice, and 34% in 19-month-old mice (Figures 3E and 3F). Intriguingly,

(B) Percentage of each ependymal cell subtype and state in the integrated scRNA-seq dataset.
(C) Expression distribution of selected marker genes.
(D) Ependymal cell subtype-specific expression of key marker genes using RNAscope. Insets, close-up views of representative cells of each subtype in (A). Note that cells outside the central canal also express some of the ependymal subtype-specific markers (Figure S3A). Scale bars, 20 and 5 μm (insets).
(E) Quantification of the percentage of ependymal cells expressing the gene markers shown in (D) and their location within the ependymal layer (n = 3–4 mice for each marker combination and 3–6 sections per mouse). Asterisks highlight cells expressing ependymal subtype-specific markers outside of the central canal.
(F) Selected GO biological processes significantly overrepresented in each ependymal cell subtype ranked by adjusted p value (FDR). Asterisk in the lateral activated cell state in (A) and (C) cautions that we did not find ependymal cells expressing high levels of *Fos* in the intact spinal cord (Figure S4).

Please cite this article in press as: Rodrigo Albors et al., An ependymal cell census identifies heterogeneous and ongoing cell maturation in the adult mouse spinal cord that changes dynamically on injury, Developmental Cell (2023), https://doi.org/10.1016/j.devcel.2023.01.003

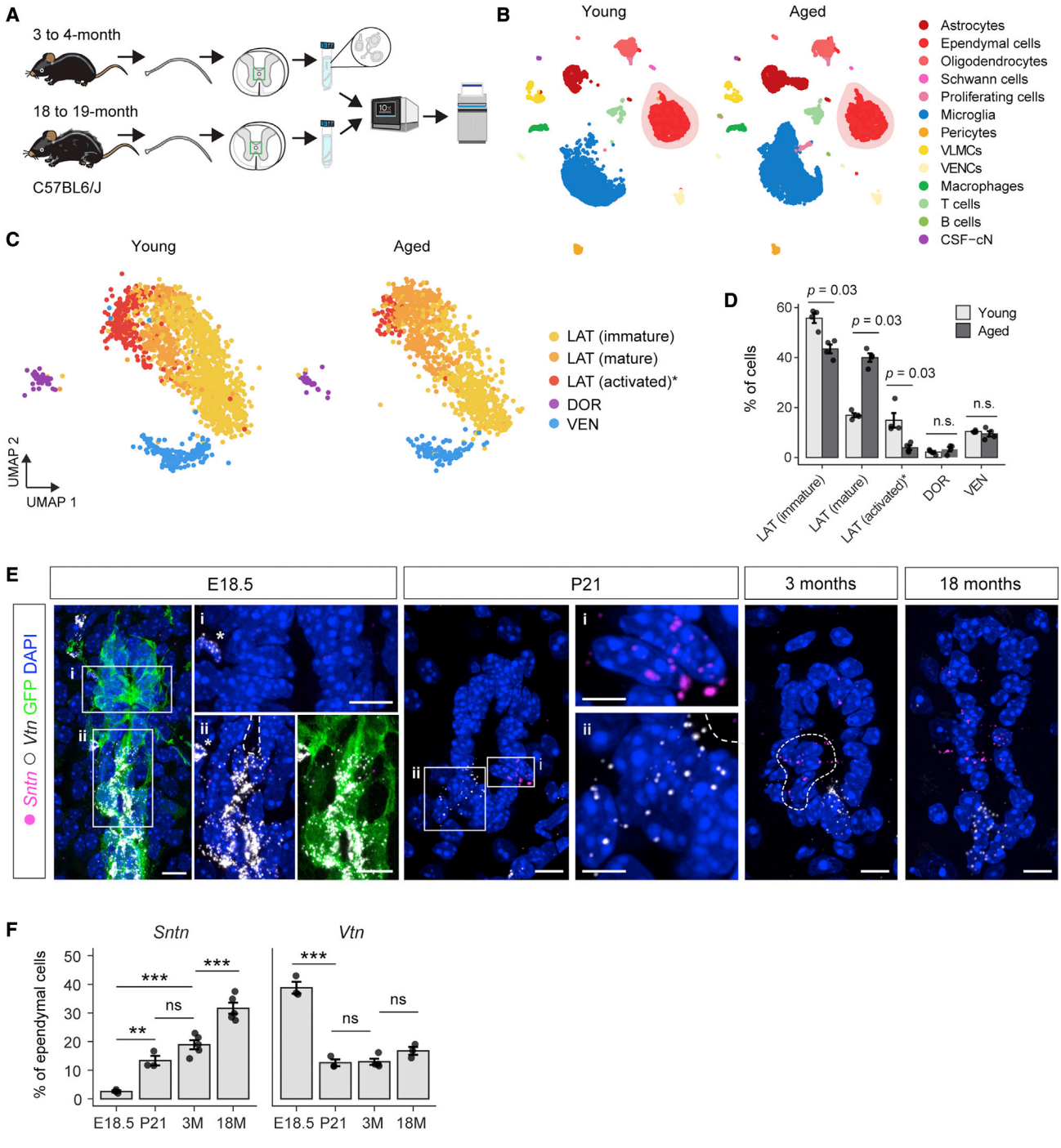

Figure 3. Age-related changes in spinal cord ependymal cells

(A) Workflow for the generation of the aging dataset.

(B) UMAP plot of spinal cord ependymal cells split by age and colored by major cell types.

(C) UMAP plot of ependymal cell subtypes and states from young and aged mice. LAT, lateral; DOR, dorsal; VEN, ventral. The asterisk next to the activated cell state indicates that this subpopulation expresses high levels of stress-related genes and that such cells are lacking in the intact spinal cord (Figure S4).

(D) Percentage of each ependymal cell subtype and state in young and aged mice. Each dot represents one mouse (n = 4 mice). Bars indicate the mean; error bars, standard deviation (SD); Wilcoxon rank-sum test (**p < 0.01, ***p < 0.001, n.s. not significant).

(E) Expression of *Sntn* and *Vtn* in E18.5 embryos, P21 pups, 3- and 18-month-old mice. Images are a maximum intensity projection (MPI) of 3–5 optical z slices encompassing a cell length. The E18.5 image additionally shows GFP expression under the control of the human *FOXJ1* promoter to highlight ependymal cells. The dashed line in the image from the 3-month-old mouse encircles a cluster of *Sntn* cells. Scale bars, 20 and 5 μm (high-magnification images).

(F) Quantification of the percentage of ependymal cells expressing *Sntn* and *Vtn* across ages. Each dot represents one mouse (n = 4 mice). Bars indicate the mean; error bars, SD; one-way ANOVA with Tukey's multiple comparisons test (**p < 0.01, ***p < 0.001, n.s. not significant).

Please cite this article in press as: Rodrigo Albors et al., An ependymal cell census identifies heterogeneous and ongoing cell maturation in the adult mouse spinal cord that changes dynamically on injury, Developmental Cell (2023), https://doi.org/10.1016/j.devcel.2023.01.003

CellPress
OPEN ACCESS

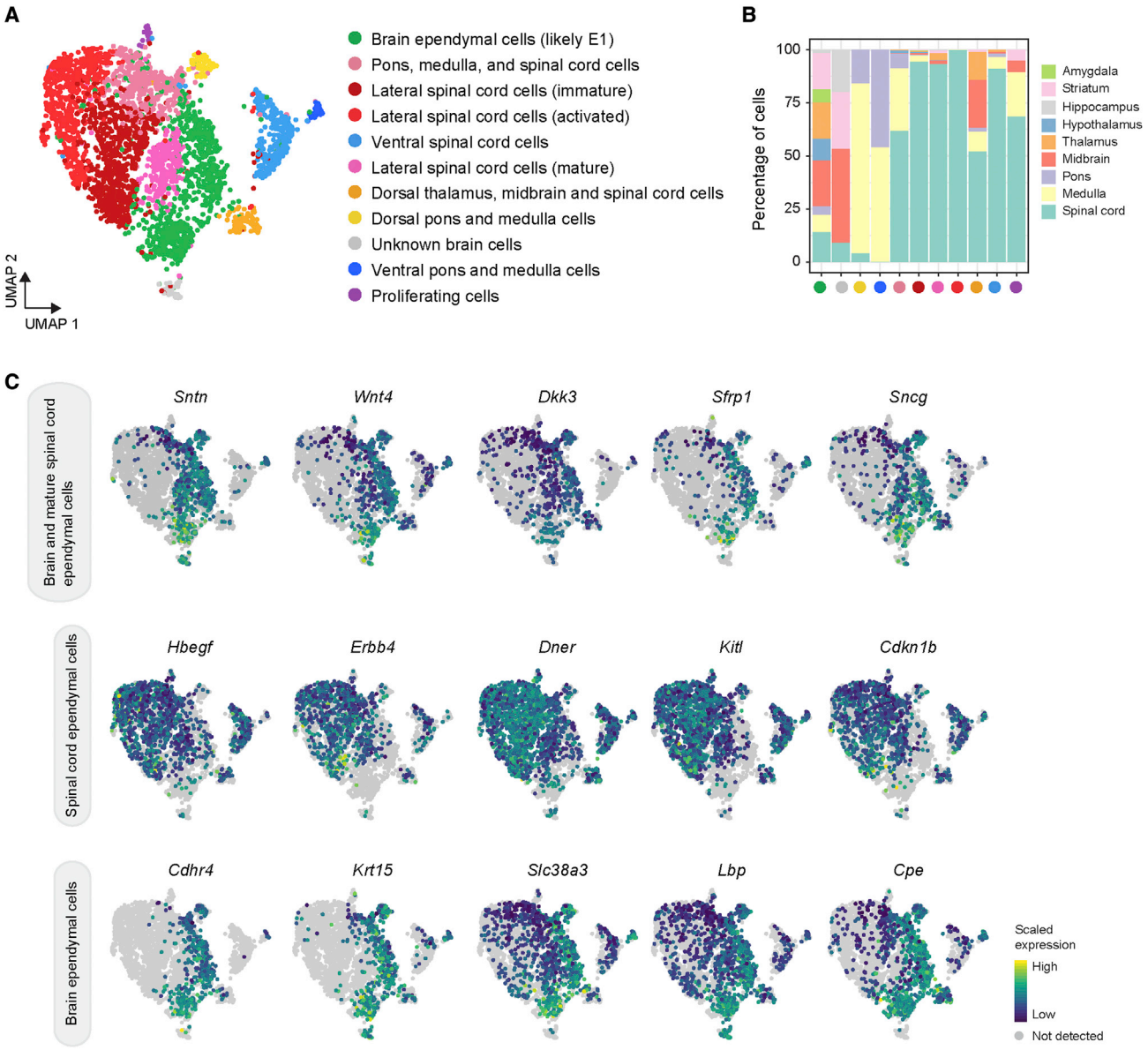

Figure 4. Ependymal cell heterogeneity across the CNS

(A) UMAP plot of ependymal cells across the CNS, including cells from our 10x dataset from young mice and from Zeisel et al.[38]

(B) Percentage of cells within each cluster from each tissue. Dots color-coded to represent ependymal subtype as in (A).

(C) Expression distribution of key genes.

Sntn-expressing cells often appeared clustered (Figure 3E). By comparison, the percentage of cells expressing the ventral-specific marker *Vtn* did not significantly change postnatally (Figures 3D and 3E). Taken together, this analysis reveals that the lateral ependymal cell population gradually adopts a more mature cell state, indicating that ependymal cell maturation in the spinal cord is ongoing throughout life.

Sntn spinal cord ependymal cells are transcriptionally similar to postmitotic brain ependymal cells

Although some spinal cord ependymal cells proliferate and can generate specialized cells in response to injury,[11,21,33] brain ependymal cells are postmitotic and cannot function as neural stem cells even though some appear to transform into neuroblasts following stroke.[6,7,11,21,33,74] To uncover transcriptomic differences that map to these important differences between the spinal cord and brain ependymal cells, we integrated our 10x ependymal cell dataset from young adult mice with published ependymal cell transcriptomes from across the CNS[38] (Figures 4A, 4B, S6A, and S6B). The integrated dataset split into 15 clusters (Figures S6C and S6D) that we manually merged into 11 clusters based on their gene expression profile, known ependymal subtypes, and region of origin (Figures 4A and 4B). Visualizing how cell populations diverge with increasing

Please cite this article in press as: Rodrigo Albors et al., An ependymal cell census identifies heterogeneous and ongoing cell maturation in the adult mouse spinal cord that changes dynamically on injury, Developmental Cell (2023), https://doi.org/10.1016/j.devcel.2023.01.003

clustering resolution, we noticed that the mature spinal cord cell cluster arose from within the brain ependymal cell "branch" (Figure S6C). This suggests that mature spinal cord cells are transcriptionally similar to brain ependymal cells. Indeed, *Sntn* and other genes expressed by mature spinal cord ependymal cells were expressed by nearly all brain ependymal cells (Figure 4C; Table S5). The fact that ependymal cells in the mouse brain complete their maturation during the first two postnatal weeks[6] further supports the idea that *Sntn* marks mature ependymal cells. Moreover, genes enriched in brain ependymal cells were associated with GO terms overrepresented in mature spinal cord cells and in spinal cord ependymal cells from aged mice (e.g., mitochondrial function and cilia) (Table S5). These predicted functional similarities between brain ependymal cells and *Sntn* spinal cord ependymal cells suggest that the latter represent a mature cell state and further support the observation that lateral spinal cord ependymal cells mature much more slowly than their brain counterparts.

Perhaps not surprisingly given their distinct embryonic origins in the anterior neural plate and the posterior neural plate/neuromesodermal progenitors,[6,75–78] brain and spinal cord ependymal cells, including mature cells, also exhibited marked molecular differences (Figure 4C). Wnt/β-catenin signaling plays a key role in spinal cord ependymal cell proliferation.[49,50] Interestingly, brain ependymal cells uniquely expressed *Sfrp1*, a secreted protein that blocks the interaction between Wnt ligands and their receptors and actively maintains quiescence in the subventricular zone[79] (Figure 4C). This identifies the distinct regulation of Wnt signaling as a potential explanation for differences in the maturation and proliferative capacity of the brain and spinal cord ependymal cells. We also identified genes unique to spinal cord ependymal cells that indicate distinct signaling capabilities in the central canal niche. These include the growth factor *Hbegf* and its potential receptor tyrosine kinase *Erbb4* (Figure 4C). Additionally, spinal cord ependymal cells uniquely express *Cdkn1b*. By contrast, genes enriched in brain ependymal cells were related to cell adhesion (e.g., *Cdhr4* and *Dchs1*), cytoskeleton (e.g., *Krt15* and *Sncg*), transport (e.g., *Slc38a3*), innate immune response (e.g., *Lbp*), and hormone metabolism (e.g., *Cpe*). These comparisons provide further evidence for protracted maturation in spinal cord ependymal cells and highlight the maintenance of a more dynamic signaling microenvironment in the spinal cord. This raises the intriguing possibility that the range of maturation states within the spinal cord central canal underlies the ability of this cell population to respond to injury, whereas this ability is lost as cells mature.

Lateral ependymal cell maturation is reversible but quickly regained in the injured spinal cord

To test whether mature spinal cord ependymal cells represent a terminally differentiated cell state we investigated how these cells respond to a challenge using an *ex vivo* model of spinal cord injury.[80] Briefly, we generated spinal cord slices from 5-month-old mice and immediately fixed some to define intact spinal cord conditions (day 0) while we cultured others for 3 and 5 days to explore whether *Sntn*-expressing cells proliferate in this context (Figure 5A). For this, we combined RNAscope for *Sntn* and the ependymal-enriched gene *Mia* with immunofluorescence for the cell proliferation marker Ki67. In the intact spinal cord, 25% of ependymal cells expressed *Sntn*, and most appeared in clusters (Figures 5B and 5C). Of the few ependymal cells that we found proliferating in the intact spinal cord (3/862 or 0.4% of ependymal cells), none expressed *Sntn* (Figures 5B and 5C). After 3 days, ependymal cell proliferation increased sharply (40% of the cells), whereas the fraction of *Sntn*-expressing cells decreased significantly compared with normal conditions (from 25% to 14%) (Figures 5B and 5C). This suggested that either *Sntn*-expressing cells are preferentially lost following injury or that, despite the expression of this mature cell marker, such cells remain plastic and can downregulate *Sntn*. In support of such cell plasticity, we found that the percentage of low-level expressing *Sntn* cells was higher in cultured spinal cord slices than in the intact spinal cord (Figure 5C). This suggests that *Sntn* expression is indeed dynamically regulated. Importantly, most Ki67-positive ependymal cells were *Sntn*-negative, but a small fraction expressed low-level *Sntn* (Figures 5B and 5C). We did not find cells expressing high levels of *Sntn* proliferating in the injured spinal cord (Figure 5B). These findings suggest that *Sntn* expression is dynamically regulated in some but perhaps not all mature lateral cells and that *Sntn* downregulation (i.e., maturation reversal) is correlated with cell cycle re-entry. Strikingly, in spinal cord slices cultured for 5 days, the percentage of *Sntn*-expressing cells and proliferating cells returned close to those under normal conditions (26% and 0.8%, respectively), and *Sntn* cells re-appeared in their characteristic clustered configuration (Figure 5B). Proliferating cells were again rare (6/727 ependymal cells), but a few expressed low levels of *Sntn* (2/6 proliferating cells or 33%) (Figures 5B and 5C). None of the cells expressing high levels of *Sntn* were proliferating.

To assess whether the ependymal cell response *ex vivo* recapitulates that observed following spinal cord injury *in vivo*, we permanently labeled ependymal cells in age-matched Foxj1-CreER^{T2}-tdTomato (Foxj1-tdTomato) mice before performing a dorsal funiculus incision injury. Strikingly, the expression dynamics of *Sntn* and Ki67 at the lesion core matched well with that observed in our *ex vivo* assay (Figure 5). The fraction of *Sntn*-expressing cells was close to 80% lower 3 dpi (from 25% to 6% of ependymal cells), whereas the fraction of Ki67-positive cells peaked (35% of ependymal cells) before both the fraction of *Sntn* and proliferating cells returned to basal levels 5 dpi (30% and 2%, respectively) (Figures 5D and 5E). This comparison indicates that the simple *ex vivo* model of spinal cord injury captures similar cell behaviors and differentiation dynamics to those operating immediately after injury *in vivo*.

These findings reveal that in response to injury, the reversal of ependymal cell maturation (*Sntn* downregulation) is accompanied by cell cycle re-entry of *Sntn*-negative cells and perhaps some low-level *Sntn*-expressing cells. As Wnt/β-catenin signaling promotes ependymal cell proliferation[49,50] and mature ependymal cells express the negative Wnt regulator *Dkk3* and non-canonical *Wnt4* (Figure 2C), this raises the possibility that mature cells normally exert an inhibitory influence on their immature neighbors.

Ependymal cells in the adult human spinal cord express *SNTN* and change their identity with age

To determine the relevance of our findings in mice to humans, we studied *SNTN* expression in 16 human spinal cord samples (years 20–29, 30–39, 40–49, and 50–59) (Table S6). We used FOXJ1 immunofluorescence to identify ependymal cells and

Please cite this article in press as: Rodrigo Albors et al., An ependymal cell census identifies heterogeneous and ongoing cell maturation in the adult mouse spinal cord that changes dynamically on injury, Developmental Cell (2023), https://doi.org/10.1016/j.devcel.2023.01.003

CellPress
OPEN ACCESS

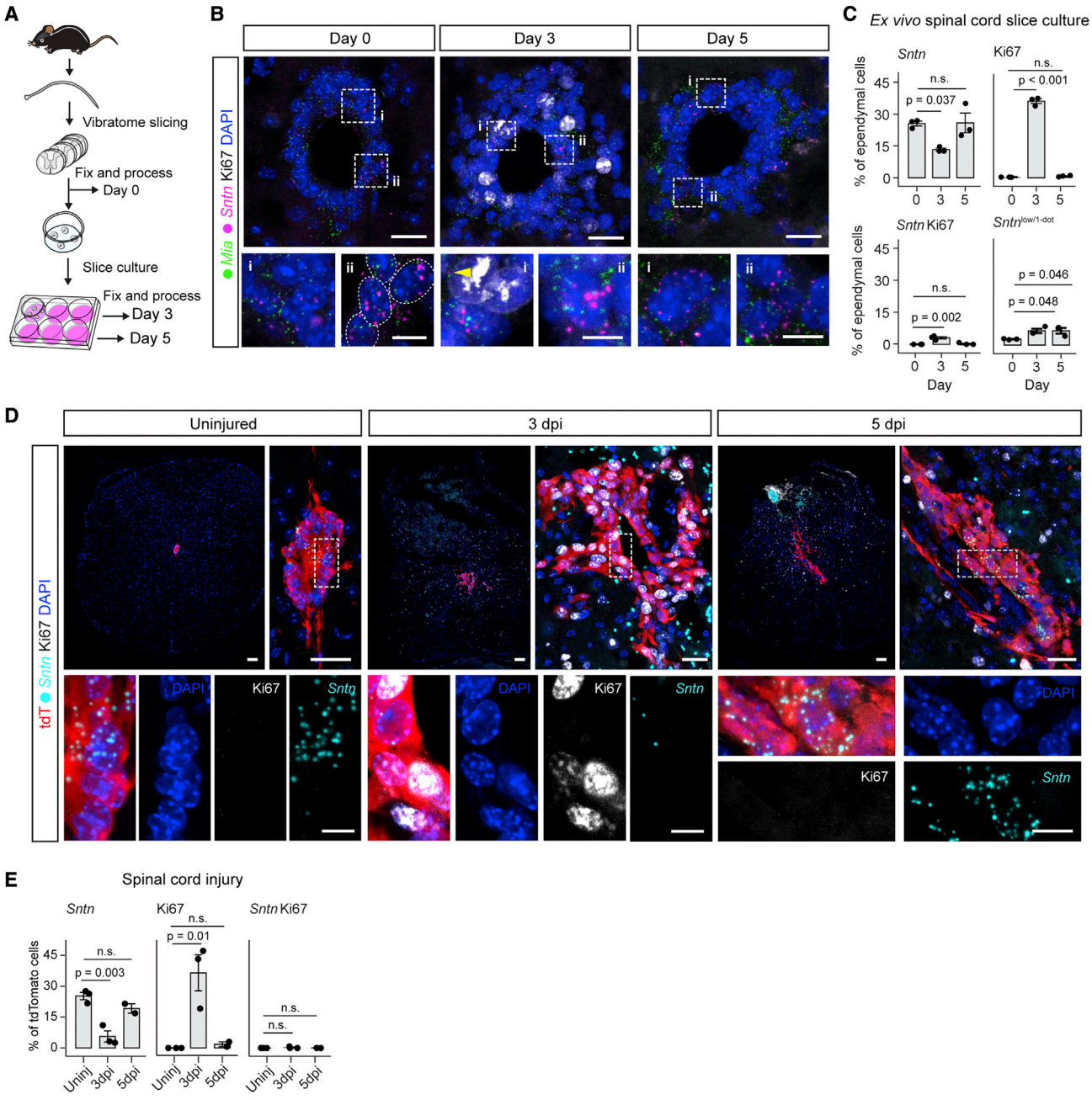

Figure 5. Downregulation of *Sntn* correlates with cell cycle re-entry in response to injury

(A) Workflow of spinal cord slice culture experiments.

(B) *Mia* and *Sntn* RNAscope and Ki67 immunofluorescence on spinal cord slices fixed immediately, at days 3 and 5 of culture.

(C) Quantification of ependymal cells expressing *Sntn*, Ki67, *Sntn* and Ki67, and *Sntn* at low level (one RNAscope dot) at days 0, 3, and 5 of culture. Each dot represents one mouse and one experiment (n = 3 mice).

(D) Uninjured and injured spinal cord of Foxj1-tdTomato mice 3 and 5 days post-injury (dpi) showing ependymal cells and their migrating progeny expressing tdTomato, *Sntn*-expressing cells, and Ki67-positive cells. A close-up view of the ependymal region is shown next to low-magnification images of the spinal cord. Boxed areas are shown below for each condition at higher magnification. Images are composites.

(E) Quantification of *Sntn* ependymal cells, Ki67 ependymal cells, *Sntn* Ki67 double-positive ependymal cells, and of cells expressing low-level *Sntn* (one RNAscope dot) in the uninjured spinal cord and at the lesion core of the injured spinal cord, 3 and 5 dpi. Each dot represents one mouse and one experiment (n = 3 mice for uninjured and 3 dpi samples, 1 mouse for 5 dpi sample). Bars indicate the mean; error bars, SD; one-way ANOVA with Dunnett's test (**p < 0.01, ***p < 0.001, n.s. not significant). All images are MIP of 2–3 optical z slices, about one cell length. Scale bars: 30 and 10 μm (higher magnification images) in (B); 50 μm (low-magnification images) in (C); and 25 μm (images of the ependymal region) and 5 μm (high-magnification images).

Please cite this article in press as: Rodrigo Albors et al., An ependymal cell census identifies heterogeneous and ongoing cell maturation in the adult mouse spinal cord that changes dynamically on injury, Developmental Cell (2023), https://doi.org/10.1016/j.devcel.2023.01.003

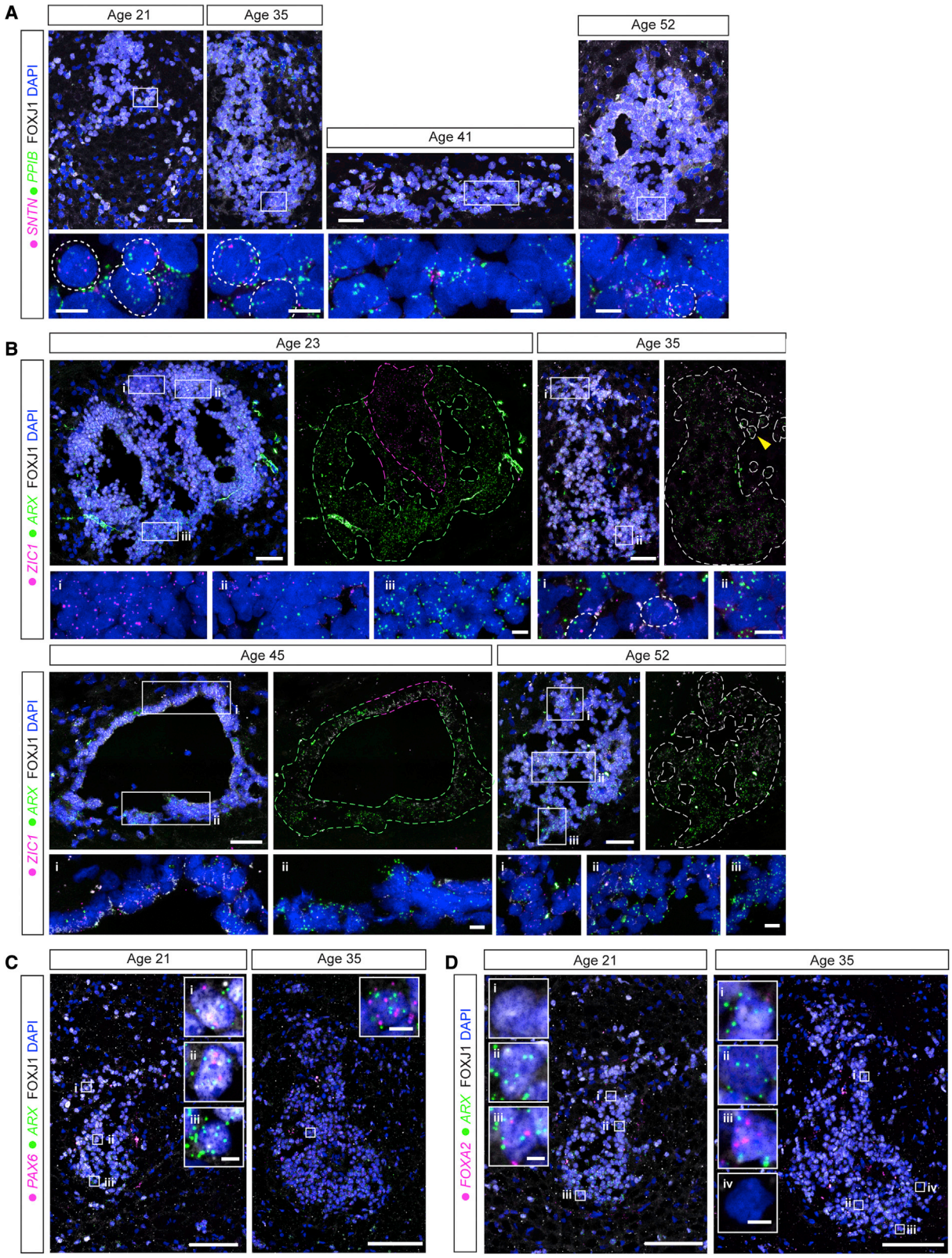

Figure 6. Ependymal cell identities in the human spinal cord

(A) Ependymal region from the human spinal cord across ages, showing combined *SNTN* and *PPIB* RNAscope and FOXJ1 immunofluorescence. High-magnification images of regions indicated in their respective low-magnification images, with dashed lines delineating individual nuclei.

(legend continued on next page)

Please cite this article in press as: Rodrigo Albors et al., An ependymal cell census identifies heterogeneous and ongoing cell maturation in the adult mouse spinal cord that changes dynamically on injury, Developmental Cell (2023), https://doi.org/10.1016/j.devcel.2023.01.003

RNAscope to detect expression of *SNTN* and of the broadly expressed gene *PPIB* to control for RNA quality (presence/absence of RNA in the sample) and non-specific probe binding or autofluorescence (as overlapping *SNTN* and *PPIB* signal) (Figure 6A). Across all ages, we found a disorganized ependyma and varying degrees of central canal stenosis, with more samples from young adults (years 20–29) having a patent canal (3/4 samples) (Figure 6). *SNTN* was widely expressed in all the human spinal cord samples examined (Figure 6A).

Our mouse GO analysis suggested that dorsal and ventral ependymal cells continue to act as signaling centers in the adult spinal cord and their position may also indicate if and how the central canal microenvironment and cellular composition change with age. We, therefore, performed RNAscope assays to detect transcripts for dorsal *ZIC1*-expressing and ventral *ARX*-expressing cells. We first assessed the specificity of these probes in the embryonic human spinal cord [Carnegie stage (CS 18)], where *ZIC1* and *ARX* expression domains were each restricted, as expected,[81] to the dorsal or ventral pole of the neural tube (Figure S7A). By contrast, we found near complementary *ZIC1* and *ARX* domains across all adult ages examined, with most ependymal cells expressing *ARX* and a small distinct subset expressing *ZIC1* dorsally (Figure 6B). This pattern of expression was independent of the extent of central canal stenosis. At the boundary between *ARX* and *ZIC1* domains, we often found ependymal cells co-expressing *ARX* and *ZIC1* (Figure 6B, age 35 inset). The quantification of cells expressing each marker was challenging; however, from age 30, *ZIC1* was expressed at lower levels and in fewer cells. By contrast, *ARX* was expressed consistently by most ependymal cells, with cells located ventrally expressing the highest levels (Figure 6B). To explore further this apparent ventralization of ependymal cells in humans, we analyzed the expression of another ventral marker, *FOXA2*, and the lateral ependymal cell marker *PAX6*. As expected, in the embryonic spinal cord ventral floor plate, cells co-expressed *ARX* and *FOXA2* but not *PAX6* (Figure S7B). In the adult spinal cord, however, we found few ependymal cells co-expressing *ARX* and *FOXA2* (3–4 cells per cross section), but most ependymal cells co-expressed *ARX* and *PAX6* (Figures 6C and 6D). These findings indicate a change in ependymal cell identity in the adult human spinal cord, with most cells co-expressing the ventral and lateral genes *ARX* and *PAX6*.

DISCUSSION

Our data divide mouse ependymal cells into dorsal, ventral, and lateral cell subtypes based on patterning genes that reflect embryonic origins and are likely to define functions (Figure 7A). In contrast to their brain counterparts, we find that many lateral ependymal cells persist in an immature cell state (Figure 7B), linking the range of cell maturation states to the ability of ependymal cells to react to injury. We discover that lateral cell maturation is reversible and propose that this may release neighboring cells from quiescence to respond to injury. The reversal of cell maturation is, however, short-lived, with cells rapidly re-establishing a mature cell state and returning to basal levels of cell proliferation (Figure 7C). In striking contrast to mice, we report that most ependymal cells in the adult human spinal cord express the mature cell marker *SNTN* and uniquely co-express the lateral and ventral cell markers *PAX6* and *ARX*. This study provides a resource with which to uncover the potential of different ependymal cell subtypes to drive spinal cord repair, it circumscribes lateral cells as the subpopulation that harbors the elusive neural stem cell potential and highlights the regulation of cell maturation as a key mechanism that provisions and perhaps limits response to injury in mammals. This spinal cord ependymal cell census can be explored further at https://ependymalcell.shinyapps.io/ependymal_atlas/.

A core finding from our study is that the lateral cell population shifted toward a mature state over time, but immature cells remained a significant fraction even in aged mice. This contrasts with the more rapid maturation of non-regenerative brain ependymal cells, which in mice is complete 2 weeks after birth.[6] Our findings, therefore, raised the possibility that the elusive spinal cord stem potential resides within the immature lateral cell fraction and is lost as cells fully mature. We tested this hypothesis in *ex vivo* and *in vivo* models of spinal cord injury and found that the mature spinal cord ependymal cell state is plastic, with some mature cells responding to injury and later adapting to reinstate tissue homeostasis. Consistent with this, spinal cord injury triggers the re-coupling of ependymal cells in a way that resembles neonatal connectivity.[82] Our findings also align well with scRNA-seq data from the whole mouse spinal cord following injury.[83] This study identified two ependymal cell subtypes, ependymal-A and ependymal-B, which based on *Sntn* expression, we can now identify as mature and immature lateral cells, respectively. Consistent with the regulation of cell maturation following injury, the authors also found that the expression of cilia-related genes and the fraction of ependymal-A/mature cells transiently decreases in the injured spinal cord[83] (see also Chevreau et al.[84]). Recently, further evidence for the downregulation of cilia-related genes in ependymal cells after injury was reported.[21] This study focused on a subpopulation of *Tnfrsf19* (Troy)-expressing ependymal cells, some of which display extraordinary neural stem cell capabilities *in vitro* and *in vivo*. However, consistent with the broad distribution of Troy-CreER recombined cells within the central canal, we found that cells of every ependymal subtype and state identified in our scRNA-seq dataset express *Tnfrsf19*. This indicates that Troy-CreER recombined cells include ependymal cells with different identities,

(B) Ependymal region from the human spinal cord across ages, showing combined RNAscope against *ZIC1* and *ARX* and FOXJ1 immunofluorescence. Colored dashed lines delineate the ependymal region and mark the distinct domains. Arrowhead in sample age 35 points to a few ependymal cells expressing *ARX* that have detached from the main cluster of ependymal cells as reported earlier.[14,29] High-magnification images show the regions indicated in their respective low-magnification images.

(C) Ependymal region from the human spinal cord showing RNAscope for *PAX6* and *ARX* and FOXJ1 immunofluorescence.

(D) Ependymal region from the human spinal cord showing RNAscope for *FOXA2* and *ARX* and FOXJ1 immunofluorescence. DNA is stained with DAPI. All images are MIP of 5–6 optical z slices, about one cell length. Low-magnification images are composites. Scale bars: 50 and 10 μm in (A) and (B) and 100 and 5 μm (lower and higher magnification images) in (C) and (D), respectively. Details about the samples analyzed can be found in Table S6.

Please cite this article in press as: Rodrigo Albors et al., An ependymal cell census identifies heterogeneous and ongoing cell maturation in the adult mouse spinal cord that changes dynamically on injury, Developmental Cell (2023), https://doi.org/10.1016/j.devcel.2023.01.003

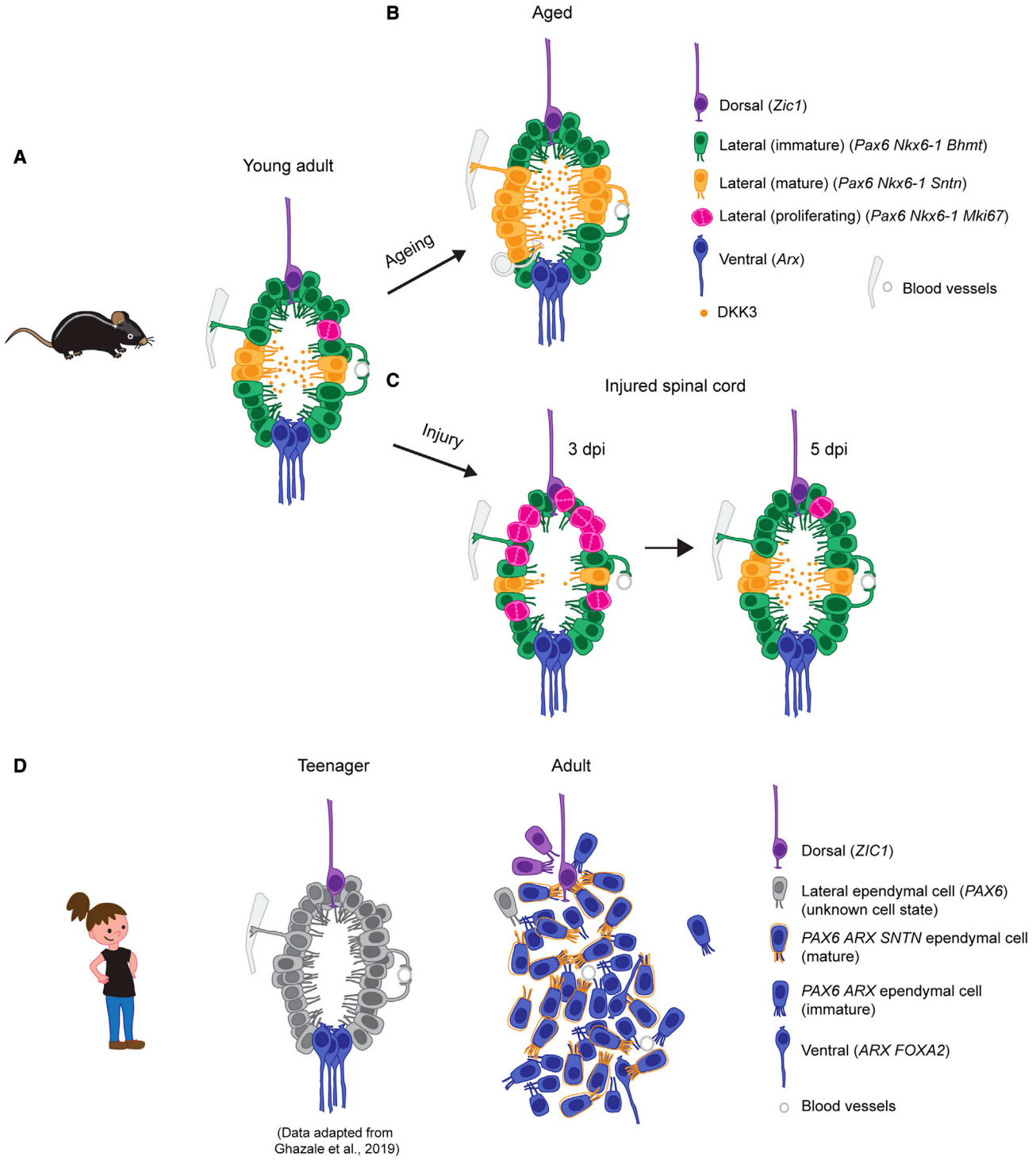

Figure 7. Schematic of key findings and model

(A) Ependymal cell subtypes in the adult mouse spinal cord. Mature lateral cells often appear clustered and express *Dkk3*, encoding a secreted negative regulator of Wnt signaling.

(B) Ongoing cell maturation is the main age-related change in the spinal cord ependymal cell population. We hypothesize that, with increasing numbers of mature cells, increased levels of secreted DKK3 protein in the central canal niche may explain the age-related decline in ependymal cell proliferation and spinal cord stem cell potential.

(legend continued on next page)

Please cite this article in press as: Rodrigo Albors et al., An ependymal cell census identifies heterogeneous and ongoing cell maturation in the adult mouse spinal cord that changes dynamically on injury, Developmental Cell (2023), https://doi.org/10.1016/j.devcel.2023.01.003

and although it is possible that Troy marks neural stem cells within each ependymal subtype, it remains unclear whether this is the case or if only a subset possess neural stem cell properties.

As many lateral ependymal cells are immature in the adult spinal cord these are likely to be the cells that mount a stem cell-like response to injury. However, the downregulation of *Sntn* in some mature cells clearly links the regulation of cell maturation to this response. In unchallenged conditions, mature cells appear in clusters and, in addition to *Sntn*, express *Dkk3*, encoding a secreted Wnt antagonist, and *Wnt4*, a non-canonical Wnt ligand. As Wnt/β-catenin signaling regulates ependymal cell proliferation,[49,50,85] these findings suggest that mature cells locally inhibit Wnt/β-catenin signaling and may thereby induce quiescence in neighboring cells, whereas their dedifferentiation may derepress Wnt/β-catenin and liberate neural stem cell behavior. This scenario could explain how neural stem cell potential is lost with increasing mature cell numbers and deeper quiescence that comes with age, and local inhibition *in vivo* may also explain the greater neural stem cell abilities that spinal cord ependymal cells display *in vitro*. Importantly, similar mechanisms operate in various stem cell niches: in the subventricular zone, *Dkk3* inhibits Wnt/β-catenin signaling[68] and WNT4 contributes to the regulation of neural stem cell quiescence;[70] WNT4 also induces muscle stem cell quiescence.[69,86] Investigating the fine-tuning of Wnt signaling in the central canal niche will be key for understanding how the balance between self-renewal and quiescence is regulated in ependymal cells. When this balance is lost, uncontrolled ependymal cell proliferation can lead to cancer tumors termed ependymoma.[87,88] Understanding how ependymal cell proliferation is kept in check may thus inform directed regenerative therapies and also cancer treatments.

Ependymal cells in the human spinal cord appear to retain dorsoventral patterning information as in the mouse; however, this was observed in just one, teenage, sample.[36] Based on *SNTN* expression, we show that most ependymal cells in the human spinal cord from age 20 are in a mature state (Figure 6A). This correlates with the apparent lack of ependymal cell proliferation in the adult human spinal cord.[14,29] Unexpectedly, we found that ventral and dorsal markers, *ARX* and *ZIC1*, are expressed in abutting domains in the adult human central canal. This contrasts strikingly with expression patterns in the adult mouse (Figure 3D) and suggests that ependymal cell identities in the adult human spinal cord fundamentally change with age. Intriguingly, spinal cord ependymal cells in the lizard do not retain dorsoventral patterning genes either and display a ventral identity.[89,90] This leads to imperfect regeneration when lizards lose their tails, as the spinal cord and surrounding tissues regrow with only ventral character due to the restricted potential of lizard ependymal cells and the signaling microenvironment they create.[89,90] Our findings raise intriguing questions about how cell maturation and changes in cell identity alter ependymal cell potential and the signaling microenvironment in the human spinal cord. In mice, chromatin accessibility for a latent oligodendrocyte program can be used to direct some ependymal cells toward an oligodendrocyte cell fate in the injured spinal cord,[20] demonstrating that ependymal cells can be manipulated to generate other cell types. It is now important to investigate whether this window of opportunity is lost with cell maturation. The spinal cord ependymal cell resource presented here can also be leveraged to inform the manipulation of distinct ependymal cell subtypes for therapeutic effect.

Limitations of the study

Ependymal cells represent a very small fraction of spinal cord cells, and some subtypes, especially dorsal and proliferating ependymal cells, are rare. The low number of dorsal cells that we captured may not provide their full transcriptomic profile due to the sparsity of 10x data. Even though our analysis identifies known and new dorsal gene markers, differential expression analysis testing may be underpowered/not have identified all significantly enriched genes. Our conclusions are based on snapshots of ependymal cells at different ages or times. To understand precisely the neural stem cell potential of distinct ependymal subtypes, it is necessary to genetically label such cells and follow their behavior during homeostasis and in response to injury. A more comprehensive characterization of human ependymal cells is necessary to assess the implications of the age-related molecular changes that we uncover. A potential limitation in studying ependymal cells in the human spinal cord is the technical differences between samples related to the lack of standardized sample collection, post-mortem time until sample collection, and varied clinical histories.

STAR★METHODS

Detailed methods are provided in the online version of this paper and include the following:

- KEY RESOURCES TABLE
- RESOURCE AVAILABILITY
  - Lead contact
  - Materials availability
  - Data and code availability
- EXPERIMENTAL MODEL AND SUBJECT DETAILS
  - Animals
  - Human samples
- METHOD DETAILS
  - Cell preparation for scRNA-seq
  - Single-cell library preparation and sequencing
  - scRNA-seq data preprocessing
  - scRNA-seq quality control, normalization, and dimensionality reduction
  - Ependymal cell heterogeneity analysis
  - Ependymal cell ageing analysis

(C) Injury triggers the reversal of ependymal cell maturation and a sharp increase in cell proliferation. However, this reversal is transient, and both the fraction of mature cells and cell proliferation quickly return to basal levels. This suggests a model in which mature cells locally repress neural stem cell abilities in their immature neighbors.
(D) In humans, ependymal cell maturation is widespread and most ependymal cells co-express the ventral and lateral markers *ARX* and *PAX6*. dpi, days post-injury.

SUPPLEMENTAL INFORMATION

Supplemental information can be found online at https://doi.org/10.1016/j.devcel.2023.01.003.

ACKNOWLEDGMENTS

We are grateful to Elly Tanaka for the critical reading of this manuscript. We are also grateful to Rosie Clarke and Arlene Rennie from the Flow Cytometry and Cell Sorting Facility at the University of Dundee for their expert FACS assistance; the WBRUTG team for technical assistance; Paul Appleton and the Dundee Imaging Facility for microscopy assistance; Edinburgh Genomics for sequencing during the COVID-19 pandemic; Jeanette Baran-Gale for very helpful and stimulating discussions on scRNA-seq data analysis; Franz Gruber for their help with all-things R and setting up the interactive web browser to explore scRNA-seq datasets; and Geoff Barton for lending A.R.A. a desk in Computational Biology. We gratefully acknowledge the Chan Zuckerberg Biohub for support and for sequencing, Foad Green, Steven Chen, Ashley Maynard, Rene Sit, Norma Neff, Spyros Darmanis, and members of the Tabula Muris Consortium for technical assistance. This project was supported by the Wellcome Trust (Wellcome Investigator award WT102817AIA to K.G.S.) and a Wings for Life grant (WFL-UK-24/17 Proj 171) to K.G.S. This project and A.R.A. were also supported by the European Union's Horizon 2020 Marie Skłodowska-Curie grant agreement no. 753812. A.R.A. was also supported by the Wellcome ISSF COVID-19 Research Momentum fund (119293) and the University of Dundee. G.A.S. was supported by Wings for Life. C.P.P. was supported by the MRC (MC_UU_00007/15). A.P.M. was supported by the Chan Zuckerberg Biohub. E.L.-B. and J.F. were supported by the Swedish Research Council, Knut and Alice Wallenbergs Stiftelse, and the Swedish Cancer Foundation. The confocal microscope used for imaging was purchased with support from Wellcome Trust Multi-User Equipment grant (WT101468).

AUTHOR CONTRIBUTIONS

A.R.A. and K.G.S. conceived and designed the study. A.R.A. generated scRNA-seq data with assistance from G.A.S. A.P.M. generated Smart-seq2 libraries and sequencing data. A.R.A. with guidance from C.P.P. performed data analysis. A.R.A. and G.A.S. generated RNAscope and immunofluorescence data from mouse and human spinal cord samples. A.R.A. and G.A.S. performed spinal cord slice culture experiments. G.A.S. and A.R.A. quantified RNAscope and immunofluorescence data. E.L.-B. with guidance from J.F. performed spinal cord injuries. A.R.A. and K.G.S. interpreted the results and wrote the original draft of the manuscript. All authors read, commented on, and proofed the final manuscript. K.G.S. and A.R.A. acquired funding.

DECLARATION OF INTERESTS

E.L.-B. and J.F. are scientific consultants to 10x Genomics.

INCLUSION AND DIVERSITY

We support inclusive, diverse, and equitable conduct of research.

Received: March 31, 2022
Revised: October 14, 2022
Accepted: January 4, 2023
Published: January 26, 2023

REFERENCES

1. Riquelme, P.A., Drapeau, E., and Doetsch, F. (2008). Brain micro-ecologies: neural stem cell niches in the adult mammalian brain. Philos. Trans. R. Soc. Lond. B Biol. Sci. *363*, 123–137. https://doi.org/10.1098/rstb.2006.2016.
2. Hugnot, J.P., and Franzen, R. (2011). The spinal cord ependymal region: a stem cell niche in the caudal central nervous system. Front. Biosci. (Landmark Ed) *16*, 1044–1059. https://doi.org/10.2741/3734.
3. Becker, C.G., Becker, T., and Hugnot, J.-P. (2018). The spinal ependymal zone as a source of endogenous repair cells across vertebrates. Prog. Neurobiol. *170*, 67–80. https://doi.org/10.1016/j.pneurobio.2018.04.002.
4. Sabelström, H., Stenudd, M., and Frisén, J. (2013). Neural stem cells in the adult spinal cord. Exp. Neurol. *260*, 44–49. https://doi.org/10.1016/j.expneurol.2013.01.026.
5. Chiasson, B.J., Tropepe, V., Morshead, C.M., and van der Kooy, D. (1999). Adult mammalian forebrain ependymal and subependymal cells demonstrate proliferative potential, but only subependymal cells have neural stem cell characteristics. J. Neurosci. *19*, 4462–4471. https://doi.org/10.1523/JNEUROSCI.19-11-04462.1999.
6. Spassky, N., Merkle, F.T., Flames, N., Tramontin, A.D., García-Verdugo, J.M., and Alvarez-Buylla, A. (2005). Adult ependymal cells are postmitotic and are derived from radial glial cells during embryogenesis. J. Neurosci. *25*, 10–18. https://doi.org/10.1523/JNEUROSCI.1108-04.2005.
7. Shah, P.T., Stratton, J.A., Stykel, M.G., Abbasi, S., Sharma, S., Mayr, K.A., Koblinger, K., Whelan, P.J., and Biernaskie, J. (2018). Single-cell transcriptomics and fate mapping of ependymal cells reveals an absence of neural stem cell function. Cell *173*, 1045–1057.e9. https://doi.org/10.1016/j.cell.2018.03.063.
8. Doetsch, F., Caillé, I., Lim, D.A., García-Verdugo, J.M., and Alvarez-Buylla, A. (1999). Subventricular zone astrocytes are neural stem cells in the adult mammalian brain. Cell *97*, 703–716. https://doi.org/10.1016/s0092-8674(00)80783-7.
9. Capela, A., and Temple, S. (2002). LeX/ssea-1 is expressed by adult mouse CNS stem cells, identifying them as nonependymal. Neuron *35*, 865–875. https://doi.org/10.1016/s0896-6273(02)00835-8.
10. Doetsch, F., García-Verdugo, J.M., and Alvarez-Buylla, A. (1997). Cellular composition and three-dimensional organization of the subventricular germinal zone in the adult mammalian brain. J. Neurosci. *17*, 5046–5061. https://doi.org/10.1523/JNEUROSCI.17-13-05046.1997.
11. Meletis, K., Barnabé-Heider, F., Carlén, M., Evergren, E., Tomilin, N., Shupliakov, O., and Frisén, J. (2008). Spinal cord injury reveals multilineage differentiation of ependymal cells. PLoS Biol. *6*, e182. https://doi.org/10.1371/journal.pbio.0060182.
12. Barnabé-Heider, F., Göritz, C., Sabelström, H., Takebayashi, H., Pfrieger, F.W., Meletis, K., and Frisén, J. (2010). Origin of new glial cells in intact and injured adult spinal cord. Cell Stem Cell *7*, 470–482. https://doi.org/10.1016/j.stem.2010.07.014.
13. Johansson, C.B., Momma, S., Clarke, D.L., Risling, M., Lendahl, U., and Frisén, J. (1999). Identification of a neural stem cell in the adult mammalian central nervous system. Cell *96*, 25–34. https://doi.org/10.1016/s0092-8674(00)80956-3.
14. Dromard, C., Guillon, H., Rigau, V., Ripoll, C., Sabourin, J.C., Perrin, F.E., Scamps, F., Bozza, S., Sabatier, P., Lonjon, N., et al. (2008). Adult human spinal cord harbors neural precursor cells that generate neurons and glial cells in vitro. J. Neurosci. Res. *86*, 1916–1926. https://doi.org/10.1002/jnr.21646.
15. Pfenninger, C.V., Steinhoff, C., Hertwig, F., and Nuber, U.A. (2011). Prospectively isolated CD133/CD24-positive ependymal cells from the adult spinal cord and lateral ventricle wall differ in their long-term in vitro self-renewal and in vivo gene expression. Glia *59*, 68–81. https://doi.org/10.1002/glia.21077.
16. Bauchet, L., Lonjon, N., Vachiery-Lahaye, F., Boularan, A., Privat, A., and Hugnot, J.-P. (2013). Isolation and Culture of Precursor Cells from the Adult Human Spinal Cord. In Neural Progenitor Cells: Methods and

Protocols, B.A. Reynolds and L.P. Deleyrolle, eds. (Humana Press), pp. 87–93. https://doi.org/10.1007/978-1-62703-574-3_8.

17. Lacroix, S., Hamilton, L.K., Vaugeois, A., Beaudoin, S., Breault-Dugas, C., Pineau, I., Lévesque, S.A., Grégoire, C.-A., and Fernandes, K.J.L. (2014). Central canal ependymal cells proliferate extensively in response to traumatic spinal cord injury but not demyelinating lesions. PLoS One *9*, e85916. https://doi.org/10.1371/journal.pone.0085916.
18. Mothe, A.J., Zahir, T., Santaguida, C., Cook, D., and Tator, C.H. (2011). Neural stem/progenitor cells from the adult human spinal cord are multipotent and self-renewing and differentiate after transplantation. PLoS One *6*, e27079. https://doi.org/10.1371/journal.pone.0027079.
19. Li, X., Floriddia, E.M., Toskas, K., Chalfouh, C., Honore, A., Aumont, A., Vallières, N., Lacroix, S., Fernandes, K.J.L., Guérout, N., et al. (2018). FoxJ1 regulates spinal cord development and is required for the maintenance of spinal cord stem cell potential. Exp. Cell Res. *368*, 84–100. https://doi.org/10.1016/j.yexcr.2018.04.017.
20. Llorens-Bobadilla, E., Chell, J.M., Le Merre, P., Wu, Y., Zamboni, M., Bergenstråhle, J., Stenudd, M., Sopova, E., Lundeberg, J., Shupliakov, O., et al. (2020). A latent lineage potential in resident neural stem cells enables spinal cord repair. Science *370*, eabb8795. https://doi.org/10.1126/science.abb8795.
21. Stenudd, M., Sabelström, H., Llorens-Bobadilla, E., Zamboni, M., Blom, H., Brismar, H., Zhang, S., Basak, O., Clevers, H., Göritz, C., et al. (2022). Identification of a discrete subpopulation of spinal cord ependymal cells with neural stem cell properties. Cell Rep. *38*, 110440. https://doi.org/10.1016/j.celrep.2022.110440.
22. Reimer, M.M., Sörensen, I., Kuscha, V., Frank, R.E., Liu, C., Becker, C.G., et al. (2008). Motor neuron regeneration in adult zebrafish. J. Neurosci. *28*, 8510–8516. https://doi.org/10.1523/JNEUROSCI.1189-08.2008.
23. McHedlishvili, L., Epperlein, H.H., Telzerow, A., and Tanaka, E.M. (2007). A clonal analysis of neural progenitors during axolotl spinal cord regeneration reveals evidence for both spatially restricted and multipotent progenitors. Development *134*, 2083–2093. https://doi.org/10.1242/dev.02852.
24. Rodrigo Albors, A., Tazaki, A., Rost, F., Nowoshilow, S., Chara, O., and Tanaka, E.M. (2015). Planar cell polarity-mediated induction of neural stem cell expansion during axolotl spinal cord regeneration. eLife *4*, e10230. https://doi.org/10.7554/eLife.10230.
25. Becker, C.G., and Becker, T. (2015). Neuronal regeneration from ependymo-radial glial cells: cook, little pot, cook! Dev. Cell *32*, 516–527. https://doi.org/10.1016/j.devcel.2015.01.001.
26. Tazaki, A., Tanaka, E.M., and Fei, J.-F. (2017). Salamander spinal cord regeneration: the ultimate positive control in vertebrate spinal cord regeneration. Dev. Biol. *432*, 63–71. https://doi.org/10.1016/j.ydbio.2017.09.034.
27. Sabelström, H., Stenudd, M., Réu, P., Dias, D.O., Elfineh, M., Zdunek, S., Damberg, P., Göritz, C., and Frisén, J. (2013). Resident neural stem cells restrict tissue damage and neuronal loss after spinal cord injury in mice. Science *342*, 637–640. https://doi.org/10.1126/science.1242576.
28. Rolls, A., Shechter, R., and Schwartz, M. (2009). The bright side of the glial scar in CNS repair. Nat. Rev. Neurosci. *10*, 235–241. https://doi.org/10.1038/nrn2591.
29. Alfaro-Cervello, C., Cebrian-Silla, A., Soriano-Navarro, M., Garcia-Tarraga, P., Matías-Guiu, J., Gomez-Pinedo, U., Molina Aguilar, P., Alvarez-Buylla, A., Luquin, M.R., and Garcia-Verdugo, J.M. (2014). The adult macaque spinal cord central canal zone contains proliferative cells and closely resembles the human. J. Comp. Neurol. *522*, 1800–1817. https://doi.org/10.1002/cne.23501.
30. Paniagua-Torija, B., Norenberg, M., Arevalo-Martin, A., Carballosa-Gautam, M.M., Campos-Martin, Y., Molina-Holgado, E., and Garcia-Ovejero, D. (2018). Cells in the adult human spinal cord ependymal region do not proliferate after injury. J. Pathol. *246*, 415–421. https://doi.org/10.1002/path.5151.
31. Hugnot, J.-P. (2013). Isolate and Culture Neural Stem Cells from the Mouse Adult Spinal Cord. In Neural Progenitor Cells: Methods and Protocols, B.A. Reynolds and L.P. Deleyrolle, eds. (Humana Press), pp. 53–63. https://doi.org/10.1007/978-1-62703-574-3_5.
32. Barnabé-Heider, F., and Frisén, J. (2008). Stem cells for spinal cord repair. Cell Stem Cell *3*, 16–24. https://doi.org/10.1016/j.stem.2008.06.011.
33. Alfaro-Cervello, C., Soriano-Navarro, M., Mirzadeh, Z., Alvarez-Buylla, A., and Garcia-Verdugo, J.M. (2012). Biciliated ependymal cell proliferation contributes to spinal cord growth. J. Comp. Neurol. *520*, 3528–3552. https://doi.org/10.1002/cne.23104.
34. Bruni, J.E., and Reddy, K. (1987). Ependyma of the central canal of the rat spinal cord: a light and transmission electron microscopic study. J. Anat. *152*, 55–70.
35. Sabourin, J.-C., Ackema, K.B., Ohayon, D., Guichet, P.-O., Perrin, F.E., Garces, A., et al. (2009). A mesenchymal-like ZEB1 +Niche harbors dorsal radial glial fibrillary acidic protein-positive stem cells in the spinal cord. Stem Cells *27*, 2722–2733. https://doi.org/10.1002/stem.226.
36. Ghazale, H., Ripoll, C., Leventoux, N., Jacob, L., Azar, S., Mamaeva, D., Glasson, Y., Calvo, C.-F., Thomas, J.-L., Meneceur, S., et al. (2019). RNA profiling of the human and mouse spinal cord stem cell niches reveals an embryonic-like regionalization with MSX1+ roof-plate-derived cells. Stem Cell Rep. *12*, 1159–1177. https://doi.org/10.1016/j.stemcr.2019.04.001.
37. Petit, A., Sanders, A.D., Kennedy, T.E., Tetzlaff, W., Glattfelder, K.J., Dalley, R.A., Puchalski, R.B., Jones, A.R., and Roskams, A.J. (2011). Adult spinal cord radial glia display a unique progenitor phenotype. PLoS One *6*, e24538. https://doi.org/10.1371/journal.pone.0024538.
38. Zeisel, A., Hochgerner, H., Lönnerberg, P., Johnsson, A., Memic, F., van der Zwan, J., Häring, M., Braun, E., Borm, L.E., La Manno, G., et al. (2018). Molecular architecture of the mouse nervous system. Cell *174*, 999–1014.e22. https://doi.org/10.1016/j.cell.2018.06.021.
39. Blum, J.A., Klemm, S., Shadrach, J.L., Guttenplan, K.A., Nakayama, L., Kathiria, A., Hoang, P.T., Gautier, O., Kaltschmidt, J.A., Greenleaf, W.J., et al. (2021). Single-cell transcriptomic analysis of the adult mouse spinal cord reveals molecular diversity of autonomic and skeletal motor neurons. Nat. Neurosci. *24*, 572–583. https://doi.org/10.1038/s41593-020-00795-0.
40. Frederico, B., Martins, I., Chapela, D., Gasparrini, F., Chakravarty, P., Ackels, T., Piot, C., Almeida, B., Carvalho, J., Ciccarelli, A., et al. (2022). DNGR-1-tracing marks an ependymal cell subset with damage-responsive neural stem cell potential. Dev. Cell *57*, 1957–1975.e9. https://doi.org/10.1016/j.devcel.2022.07.012.
41. Fiorelli, R., Cebrian-Silla, A., Garcia-Verdugo, J.-M., and Raineteau, O. (2013). The adult spinal cord harbors a population of GFAP-positive progenitors with limited self-renewal potential. Glia *61*, 2100–2113. https://doi.org/10.1002/glia.22579.
42. Kasantikul, V., Netsky, M.G., and James, A.E., Jr. (1979). Relation of age and cerebral ventricle size to central canal in man. Morphological analysis. J. Neurosurg. *51*, 85–93. https://doi.org/10.3171/jns.1979.51.1.0085.
43. Milhorat, T.H., Kotzen, R.M., and Anzil, A.P. (1994). Stenosis of central canal of spinal cord in man: incidence and pathological findings in 232 autopsy cases. J. Neurosurg. *80*, 716–722. https://doi.org/10.3171/jns.1994.80.4.0716.
44. Yasui, K., Hashizume, Y., Yoshida, M., Kameyama, T., and Sobue, G. (1999). Age-related morphologic changes of the central canal of the human spinal cord. Acta Neuropathol. *97*, 253–259. https://doi.org/10.1007/s004010050982.
45. Torrillas de la Cal, A., Paniagua-Torija, B., Arevalo-Martin, A., Faulkes, C.G., Jiménez, A.J., Ferrer, I., Molina-Holgado, E., and Garcia-Ovejero, D. (2021). The structure of the spinal cord ependymal region in adult humans is a distinctive trait among mammals. Cells *10*, 2235. https://doi.org/10.3390/cells10092235.
46. Ostrowski, L.E., Hutchins, J.R., Zakel, K., and O'Neal, W.K. (2003). Targeting expression of a transgene to the airway surface epithelium

using a ciliated cell-specific promoter. Mol. Ther. *8*, 637–645. https://doi.org/10.1016/s1525-0016(03)00221-1.

47. Spassky, N., and Meunier, A. (2017). The development and functions of multiciliated epithelia. Nat. Rev. Mol. Cell Biol. *18*, 423–436. https://doi.org/10.1038/nrm.2017.21.
48. Bruni, J.E., Del Bigio, M.R., and Clattenburg, R.E. (1985). Ependyma: normal and pathological. A review of the literature. Brain Res. *356*, 1–19. https://doi.org/10.1016/0165-0173(85)90016-5.
49. Shinozuka, T., Takada, R., Yoshida, S., Yonemura, S., and Takada, S. (2019). Wnt produced by stretched roof-plate cells is required for the promotion of cell proliferation around the central canal of the spinal cord. Development *146*. dev159343–dev159324.
50. Xing, L., Anbarchian, T., Tsai, J.M., Plant, G.W., and Nusse, R. (2018). Wnt/β-catenin signaling regulates ependymal cell development and adult homeostasis. Proc. Natl. Acad. Sci. USA *115*, E5954–E5962. https://doi.org/10.1073/pnas.1803297115.
51. Khazanov, S., Paz, Y., Hefetz, A., Gonzales, B.J., Netser, Y., Mansour, A.A., and Ben-Arie, N. (2017). Floor plate descendants in the ependyma of the adult mouse central nervous system. Int. J. Dev. Biol. *61*, 257–265. https://doi.org/10.1387/ijdb.160232nb.
52. Cañizares, M.A., Albors, A.R., Singer, G., Suttie, N., Gorkic, M., Felts, P., and Storey, K.G. (2020). Multiple steps characterise ventricular layer attrition to form the ependymal cell lining of the adult mouse spinal cord central canal. J. Anat. *236*, 334–350. https://doi.org/10.1111/joa.13094.
53. Fu, H., Qi, Y., Tan, M., Cai, J., Hu, X., Liu, Z., Jensen, J., and Qiu, M. (2003). Molecular mapping of the origin of postnatal spinal cord ependymal cells: evidence that adult ependymal cells are derived from Nkx6.1+ ventral neural progenitor cells. J. Comp. Neurol. *456*, 237–244. https://doi.org/10.1002/cne.10481.
54. Yu, K., McGlynn, S., and Matise, M.P. (2013). Floor plate-derived sonic hedgehog regulates glial and ependymal cell fates in the developing spinal cord. Development *140*, 1594–1604. https://doi.org/10.1242/dev.090845.
55. Masahira, N., Takebayashi, H., Ono, K., Watanabe, K., Ding, L., Furusho, M., Ogawa, Y., Nabeshima, Y.-I., Alvarez-Buylla, A., Shimizu, K., et al. (2006). Olig2-positive progenitors in the embryonic spinal cord give rise not only to motoneurons and oligodendrocytes, but also to a subset of astrocytes and ependymal cells. Dev. Biol. *293*, 358–369. https://doi.org/10.1016/j.ydbio.2006.02.029.
56. Nagai, T., Aruga, J., Takada, S., Günther, T., Spörle, R., Schughart, K., and Mikoshiba, K. (1997). The expression of the mouse Zic1, Zic2, and Zic3 gene suggests an essential role for Zic genes in body pattern formation. Dev. Biol. *182*, 299–313. https://doi.org/10.1006/dbio.1996.8449.
57. Miura, H., Yanazawa, M., Kato, K., and Kitamura, K. (1997). Expression of a novel aristaless related homeobox gene 'Arx' in the vertebrate telencephalon, diencephalon and floor plate. Mech. Dev. *65*, 99–109. https://doi.org/10.1016/s0925-4773(97)00062-2.
58. Kennedy, T.E., Serafini, T., de la Torre, J.R., and Tessier-Lavigne, M. (1994). Netrins are diffusible chemotropic factors for commissural axons in the embryonic spinal cord. Cell *78*, 425–435. https://doi.org/10.1016/0092-8674(94)90421-9.
59. Surmann-Schmitt, C., Dietz, U., Kireva, T., Adam, N., Park, J., Tagariello, A., Önnerfjord, P., Heinegård, D., Schlötzer-Schrehardt, U., Deutzmann, R., et al. (2008). Ucma, a novel secreted cartilage-specific protein with implications in osteogenesis. J. Biol. Chem. *283*, 7082–7093. https://doi.org/10.1074/jbc.M702792200.
60. Willems, B.A., Furmanik, M., Caron, M.M.J., Chatrou, M.L.L., Kusters, D.H.M., Welting, T.J.M., Stock, M., Rafael, M.S., Viegas, C.S.B., Simes, D.C., et al. (2018). Ucma/GRP inhibits phosphate-induced vascular smooth muscle cell calcification via SMAD-dependent BMP signalling. Sci. Rep. *8*, 4961. https://doi.org/10.1038/s41598-018-23353-y.
61. Kubo, A., Yuba-Kubo, A., Tsukita, S., Tsukita, S., and Amagai, M. (2008). Sentan: a novel specific component of the apical structure of vertebrate motile cilia. Mol. Biol. Cell *19*, 5338–5346. https://doi.org/10.1091/mbc.e08-07-0691.
62. Stauber, M., Boldt, K., Wrede, C., Weidemann, M., Kellner, M., Schuster-Gossler, K., Kühnel, M.P., Hegermann, J., Ueffing, M., and Gossler, A. (2017). 1700012B09Rik, a FOXJ1 effector gene active in ciliated tissues of the mouse but not essential for motile ciliogenesis. Dev. Biol. *429*, 186–199. https://doi.org/10.1016/j.ydbio.2017.06.027.
63. He, M., Wu, B., Ye, W., Le, D.D., Sinclair, A.W., Padovano, V., Chen, Y., Li, K.-X., Sit, R., Tan, M., et al. (2020). Chloride channels regulate differentiation and barrier functions of the mammalian airway. eLife *9*, e53085. https://doi.org/10.7554/eLife.53085.
64. Mali, G.R., Yeyati, P.L., Mizuno, S., Dodd, D.O., Tennant, P.A., Keighren, M.A., Zur Lage, P., Shoemark, A., Garcia-Munoz, A., Shimada, A., et al. (2018). ZMYND10 functions in a chaperone relay during axonemal dynein assembly. eLife *7*, e34389. https://doi.org/10.7554/eLife.34389.
65. Konishi, S., Gotoh, S., Tateishi, K., Yamamoto, Y., Korogi, Y., Nagasaki, T., Matsumoto, H., Muro, S., Hirai, T., Ito, I., et al. (2016). Directed induction of functional multi-ciliated cells in proximal airway epithelial spheroids from human pluripotent stem cells. Stem Cell Rep. *6*, 18–25. https://doi.org/10.1016/j.stemcr.2015.11.010.
66. Kawase, T., Ohki, R., Shibata, T., Tsutsumi, S., Kamimura, N., Inazawa, J., Ohta, T., Ichikawa, H., Aburatani, H., Tashiro, F., et al. (2009). PH domain-only protein PHLDA3 is a p53-regulated repressor of Akt. Cell *136*, 535–550. https://doi.org/10.1016/j.cell.2008.12.002.
67. Ohki, R., Saito, K., Chen, Y., Kawase, T., Hiraoka, N., Saigawa, R., Minegishi, M., Aita, Y., Yanai, G., Shimizu, H., et al. (2014). PHLDA3 is a novel tumor suppressor of pancreatic neuroendocrine tumors. Proc. Natl. Acad. Sci. USA *111*, E2404–E2413. https://doi.org/10.1073/pnas.1319962111.
68. Zhu, Y., Demidov, O.N., Goh, A.M., Virshup, D.M., Lane, D.P., and Bulavin, D.V. (2014). Phosphatase WIP1 regulates adult neurogenesis and WNT signaling during aging. J. Clin. Invest. *124*, 3263–3273. https://doi.org/10.1172/JCI73015.
69. Eliazer, S., Muncie, J.M., Christensen, J., Sun, X., D'Urso, R.S., Weaver, V.M., and Brack, A.S. (2019). Wnt4 from the niche controls the Mechano-properties and quiescent state of muscle stem cells. Cell Stem Cell *25*, 654–665.e4. https://doi.org/10.1016/j.stem.2019.08.007.
70. Chavali, M., Klingener, M., Kokkosis, A.G., Garkun, Y., Felong, S., Maffei, A., and Aguirre, A. (2018). Non-canonical Wnt signaling regulates neural stem cell quiescence during homeostasis and after demyelination. Nat. Commun. *9*, 36. https://doi.org/10.1038/s41467-017-02440-0.
71. Llorens-Bobadilla, E., Zhao, S., Baser, A., Saiz-Castro, G., Zwadlo, K., and Martin-Villalba, A. (2015). Single-cell transcriptomics reveals a population of dormant neural stem cells that become activated upon brain injury. Cell Stem Cell *17*, 329–340. https://doi.org/10.1016/j.stem.2015.07.002.
72. Shin, J., Berg, D.A., Zhu, Y., Shin, J.Y., Song, J., Bonaguidi, M.A., Enikolopov, G., Nauen, D.W., Christian, K.M., Ming, G.-L., et al. (2015). Single-Cell RNA-Seq with Waterfall Reveals Molecular Cascades underlying Adult Neurogenesis. Cell Stem Cell *17*, 360–372. https://doi.org/10.1016/j.stem.2015.07.013.
73. Li, X., Floriddia, E.M., Toskas, K., Fernandes, K.J.L., Guérout, N., and Barnabé-Heider, F. (2016). Regenerative potential of ependymal cells for spinal cord injuries over time. EBioMedicine *13*, 55–65. https://doi.org/10.1016/j.ebiom.2016.10.035.
74. Carlén, M., Meletis, K., Göritz, C., Darsalia, V., Evergren, E., Tanigaki, K., Amendola, M., Barnabé-Heider, F., Yeung, M.S.Y., Naldini, L., et al. (2009). Forebrain ependymal cells are Notch-dependent and generate neuroblasts and astrocytes after stroke. Nat. Neurosci. *12*, 259–267. https://doi.org/10.1038/nn.2268.
75. Merkle, F.T., Tramontin, A.D., García-Verdugo, J.M., and Alvarez-Buylla, A. (2004). Radial glia give rise to adult neural stem cells in the subventricular zone. Proc. Natl. Acad. Sci. USA *101*, 17528–17532. https://doi.org/10.1073/pnas.0407893101.
76. Redmond, S.A., Figueres-Oñate, M., Obernier, K., Nascimento, M.A., Parraguez, J.I., López-Mascaraque, L., Fuentealba, L.C., and Alvarez-Buylla, A. (2019). Development of ependymal and postnatal neural

stem cells and their origin from a common embryonic progenitor. Cell Rep. *27*, 429–441.e3. https://doi.org/10.1016/j.celrep.2019.01.088.

77. Tzouanacou, E., Wegener, A., Wymeersch, F.J., Wilson, V., and Nicolas, J.F. (2009). Redefining the progression of lineage segregations during mammalian embryogenesis by clonal analysis. Dev. Cell *17*, 365–376. https://doi.org/10.1016/j.devcel.2009.08.002.
78. Henrique, D., Abranches, E., Verrier, L., and Storey, K.G. (2015). Neuromesodermal progenitors and the making of the spinal cord. Development *142*, 2864–2875. https://doi.org/10.1242/dev.119768.
79. Donega, V., van der Geest, A.T., Sluijs, J.A., van Dijk, R.E., Wang, C.C., Basak, O., Pasterkamp, R.J., and Hol, E.M. (2022). Single-cell profiling of human subventricular zone progenitors identifies SFRP1 as a target to reactivate progenitors. Nat. Commun. *13*, 1036. https://doi.org/10.1038/s41467-022-28626-9.
80. Fernandez-Zafra, T., Codeluppi, S., and Uhlén, P. (2017). An ex vivo spinal cord injury model to study ependymal cells in adult mouse tissue. Exp. Cell Res. *357*, 236–242. https://doi.org/10.1016/j.yexcr.2017.06.002.
81. Rayon, T., Maizels, R.J., Barrington, C., and Briscoe, J. (2021). Single-cell transcriptome profiling of the human developing spinal cord reveals a conserved genetic programme with human-specific features. Development *148*, dev199711. https://doi.org/10.1242/dev.199711.
82. Fabbiani, G., Reali, C., Valentín-Kahan, A., Rehermann, M.I., Fagetti, J., Falco, M.V., and Russo, R.E. (2020). Connexin signaling is involved in the reactivation of a latent stem cell niche after spinal cord injury. J. Neurosci. *40*, 2246–2258. https://doi.org/10.1523/JNEUROSCI.2056-19.2020.
83. Milich, L.M., Choi, J.S., Ryan, C., Cerqueira, S.R., Benavides, S., Yahn, S.L., Tsoulfas, P., and Lee, J.K. (2021). Single-cell analysis of the cellular heterogeneity and interactions in the injured mouse spinal cord. J. Exp. Med. *218*, e20210040. https://doi.org/10.1084/jem.20210040.
84. Chevreau, R., Ghazale, H., Ripoll, C., Chalfouh, C., Delarue, Q., Hemonnot-Girard, A.L., Mamaeva, D., Hirbec, H., Rothhut, B., Wahane, S., et al. (2021). RNA profiling of mouse ependymal cells after spinal cord injury identifies the oncostatin pathway as a potential key regulator of spinal cord stem cell fate. Cells *10*, 3332. https://doi.org/10.3390/cells10123332.
85. Shinozuka, T., and Takada, S. (2021). Morphological and functional changes of roof plate cells in spinal cord development. J. Dev. Biol. *9*, 30. https://doi.org/10.3390/jdb9030030.
86. Otto, A., Schmidt, C., Luke, G., Allen, S., Valasek, P., Muntoni, F., Lawrence-Watt, D., and Patel, K. (2008). Canonical Wnt signalling induces satellite-cell proliferation during adult skeletal muscle regeneration. J. Cell Sci. *121*, 2939–2950. https://doi.org/10.1242/jcs.026534.
87. Gojo, J., Englinger, B., Jiang, L., Hübner, J.M., Shaw, M.L., Hack, O.A., Madlener, S., Kirchhofer, D., Liu, I., Pyrdol, J., et al. (2020). Single-cell RNA-seq reveals cellular hierarchies and impaired developmental trajectories in pediatric ependymoma. Cancer Cell *38*, 44–59.e9. https://doi.org/10.1016/j.ccell.2020.06.004.
88. Gillen, A.E., Riemondy, K.A., Amani, V., Griesinger, A.M., Gilani, A., Venkataraman, S., Madhavan, K., Prince, E., Sanford, B., Hankinson, T.C., et al. (2020). Single-cell RNA sequencing of childhood ependymoma reveals neoplastic cell subpopulations that impact molecular classification and etiology. Cell Rep. *32*, 108023. https://doi.org/10.1016/j.celrep.2020.108023.
89. Sun, A.X., Londono, R., Hudnall, M.L., Tuan, R.S., and Lozito, T.P. (2018). Differences in neural stem cell identity and differentiation capacity drive divergent regenerative outcomes in lizards and salamanders. Proc. Natl. Acad. Sci. USA *6*. 201803780–201803710.
90. Lozito, T.P., Londono, R., Sun, A.X., and Hudnall, M.L. (2021). Introducing dorsoventral patterning in adult regenerating lizard tails with gene-edited embryonic neural stem cells. Nat. Commun. *12*, 6010. https://doi.org/10.1038/s41467-021-26321-9.
91. Schindelin, J., Arganda-Carreras, I., Frise, E., Kaynig, V., Longair, M., Pietzsch, T., Preibisch, S., Rueden, C., Saalfeld, S., Schmid, B., et al. (2012). Fiji: an open-source platform for biological-image analysis. Nat. Methods *9*, 676–682. https://doi.org/10.1038/nmeth.2019.
92. Schaum, N., Karkanias, J., Batson, J., Botvinnik, O., Chen, M.B., Chen, S., Green, F., Jones, R.C., Maynard, A., Penland, L., et al. (2018). Single-cell transcriptomics of 20 mouse organs creates a Tabula Muris. Nature *562*, 367–372. https://doi.org/10.1038/s41586-018-0590-4.
93. Zappia, L., and Oshlack, A. (2018). Clustering trees: a visualization for evaluating clusterings at multiple resolutions. GigaScience *7*, giy083. https://doi.org/10.1093/gigascience/giy083.
94. Stuart, T., Butler, A., Hoffman, P., Hafemeister, C., Papalexi, E., Mauck, W.M., III, Hao, Y., Stoeckius, M., Smibert, P., and Satija, R. (2019). Comprehensive integration of single-cell data. Cell *177*, 1888–1902.e21. https://doi.org/10.1016/j.cell.2019.05.031.
95. Kaminow, B., Yunusov, D., and Dobin, A. (2021). STARsolo: accurate, fast and versatile mapping/quantification of single-cell and single-nucleus RNA-seq data. Preprint at bioRxiv. https://doi.org/10.1101/2021.05.05.442755.
96. Raudvere, U., Kolberg, L., Kuzmin, I., Arak, T., Adler, P., Peterson, H., and Vilo, J. (2019). g:profiler: a web server for functional enrichment analysis and conversions of gene lists (2019 update). Nucleic Acids Res. *47*, W191–W198. https://doi.org/10.1093/nar/gkz369.
97. Wickham, H. (2016). ggplot2: Elegant Graphics for Data Analysis (Springer).
98. Madisen, L., Zwingman, T.A., Sunkin, S.M., Oh, S.W., Zariwala, H.A., Gu, H., Ng, L.L., Palmiter, R.D., Hawrylycz, M.J., Jones, A.R., et al. (2010). A robust and high-throughput Cre reporting and characterization system for the whole mouse brain. Nat. Neurosci. *13*, 133–140. https://doi.org/10.1038/nn.2467.
99. Baran-Gale, J., Chandra, T., and Kirschner, K. (2018). Experimental design for single-cell RNA sequencing. Brief. Funct. Genomics *17*, 233–239. https://doi.org/10.1093/bfgp/elx035.
100. Saxena, A., Wagatsuma, A., Noro, Y., Kuji, T., Asaka-Oba, A., Watahiki, A., Gurnot, C., Fagiolini, M., Hensch, T.K., and Carninci, P. (2012). Trehalose-enhanced isolation of neuronal sub-types from adult mouse brain. BioTechniques *52*, 381–385. https://doi.org/10.2144/0000113878.
101. Picelli, S., Björklund, Å.K., Faridani, O.R., Sagasser, S., Winberg, G., and Sandberg, R. (2013). Smart-seq2 for sensitive full-length transcriptome profiling in single cells. Nat. Methods *10*, 1096–1098. https://doi.org/10.1038/nmeth.2639.
102. Picelli, S., Faridani, O.R., Björklund, A.K., Winberg, G., Sagasser, S., and Sandberg, R. (2014). Full-length RNA-seq from single cells using Smart-seq2. Nat. Protoc. *9*, 171–181. https://doi.org/10.1038/nprot.2014.006.
103. Darmanis, S., Sloan, S.A., Zhang, Y., Enge, M., Caneda, C., Shuer, L.M., Hayden Gephart, M.G., Barres, B.A., and Quake, S.R. (2015). A survey of human brain transcriptome diversity at the single cell level. Proc. Natl. Acad. Sci. USA *112*, 7285–7290. https://doi.org/10.1073/pnas.1507125112.
104. Martin, M. (2011). Cutadapt removes adapter sequences from high-throughput sequencing reads. EMBnet.journal *17*, 10–12. https://doi.org/10.14806/ej.17.1.200.
105. Dobin, A., Davis, C.A., Schlesinger, F., Drenkow, J., Zaleski, C., Jha, S., Batut, P., Chaisson, M., and Gingeras, T.R. (2013). STAR: ultrafast universal RNA-seq aligner. Bioinformatics *29*, 15–21. https://doi.org/10.1093/bioinformatics/bts635.
106. McInnes, L., Healy, J., and Melville, J. (2018). UMAP: uniform manifold approximation and projection for dimension reduction. Preprint at arXiv. https://doi.org/10.48550/arXiv.1802.03426.
107. Garnier, S., Ross, N., Rudis, R., Camargo, P.A., Sciaini, M., and Scherer, C.. Viridis—colorblind-friendly color maps for R. 2021. R package. https://sjmgarnier.github.io/viridis/.

Please cite this article in press as: Rodrigo Albors et al., An ependymal cell census identifies heterogeneous and ongoing cell maturation in the adult mouse spinal cord that changes dynamically on injury, Developmental Cell (2023), https://doi.org/10.1016/j.devcel.2023.01.003

STAR★METHODS

KEY RESOURCES TABLE

REAGENT or RESOURCE	SOURCE	IDENTIFIER
Antibodies		
Chicken anti-GFP	Sigma-Aldrich	Cat#ab13970; RRID: AB_300798
Rabbit anti-FOXJ1	Sigma-Aldrich	Cat#HPA005714; RRID: AB_1078902
Rat anti-Ki67 (SolA15)	Thermo Fisher Scientific	Cat#14-5698-82; RRID: AB_10854564
Goat anti-tdTomato	SICGEN	Cat#AB8181; RRID: AB_2722750
Donkey anti-rabbit IgG (H+L) highly cross-adsorbed secondary antibody, Alexa Fluor 568	Thermo Fisher Scientific	Cat#A10042; RRID: AB_2534017
Donkey anti-Goat IgG (H+L) highly cross-adsorbed secondary antibody, Alexa Fluor 568	Thermo Fisher Scientific	Cat#A-21432; RRID: AB_2535853
Alexa Fluor 488 AffiniPure donkey anti-chicken IgY (IgG) (H+L) antibody	Jackson ImmunoResearch Labs	Cat#703-545-155; RRID: AB_2340375
Donkey anti-rat IgG H&L (Alexa Fluor® 568)	Abcam	Cat#ab175475; RRID: AB_2636887
Biological samples		
Human spinal cord	Netherlands Brain Bank	See Table S6
Human embryonic tissue	Human Developmental Biology Resource	N/A
Chemicals, peptides, and recombinant proteins		
Neurobasal™-A Medium	Thermo Fisher Scientific	Cat#10888022
B-27	Thermo Fisher Scientific	Cat#17504044
Horse serum	Thermo Fisher Scientific	Cat#16050122
Poly-L-lysine hydrobromide	Millipore Sigma	Cat#SKU-P6282
GlutaMAX™ Supplement	Thermo Fisher Scientific	Cat#35050061
HEPES Buffer 1M	Lonza	Cat#LZBE17-737E
Penicillin-streptomycin	Millipore Sigma	Cat#SKU-P0781
Myelin Removal Beads II, human, mouse, rat	Miltenyi Biotech	Cat#130-096-731
HBSS, calcium, magnesium, no phenol red	Thermo Fisher Scientific	Cat#14025050
TrypLE™ Select Enzyme (10X), no phenol red	Thermo Fisher Scientific	Cat#A1217702
Liberase TM	Merck	Cat#5401119001
DNase I	Worthington	Cat#LS002058
Bovine serum albumin	Sigma-Aldrich	Cat#A9418
4',6-Diamidino-2-Phenylindole, Dihydrochloride (DAPI)	Sigma-Aldrich	Cat#9542
Triton X-100	Promega	Cat#H5141
D-(+)-Trehalose dihydrate	Merck	Cat#T0167
Red Blood Cell Lysis	Roche	Cat#11814389001
CellTrics, 50 μm	sysmex	Cat#04-0042-2317
Pre-Separation Filter (30 μm)	Miltenyi Biotech	Cat#130-041-407
Millicell Cell Culture Insert, 30 mm, hydrophilic PTFE, 0.4 μm	Millipore Sigma	Cat#SKU-PICM0RG50
Critical commercial assays		
Chromium Next GEM Chip G Single Cell Kit	10x Genomics	Cat#1000127
Chromium Next GEM Single Cell 3' GEM, Library & Gel Bead Kit v3.1	10x Genomics	Cat#1000128
Chromium Next GEM Single Cell 3' Gel Bead Kit v3.1	10x Genomics	Cat#1000129

(*Continued on next page*)

Continued

REAGENT or RESOURCE	SOURCE	IDENTIFIER
Chromium Next GEM Single Cell 3' GEM Kit v3.1	10x Genomics	Cat#1000130
Chromium Next GEM Single Cell 3' Library Kit v3.1	10x Genomics	Cat#1000158
High Sensitivity D5000 ScreenTape	Agilent Technologies, Inc.	Cat#5067-5592
Qubit dcDNA HS assay kit	Thermo Fisher Scientific	Cat#Q32851
RNAscope® Multiplex Fluorescent Detection Kit v2	ACD	Cat#323100
RNAscope probe: Mm-Sntn-C3	ACD	Cat#574191-C3
RNAscope probe: Mm-Vtn-C3	ACD	Cat#443601-C3
RNAscope probe: Mm-Zic1	ACD	Cat#493121
RNAscope probe: Mm-Wnt4-C2	ACD	Cat#401101-C2
RNAscope probe: Mm-Fos	ACD	Cat#316921
RNAscope probe: Mm-Bhmt	ACD	Cat#876091
RNAscope probe: Mm-Dkk3	ACD	Cat#400931
RNAscope probe: Mm-Mia	ACD	Cat#498011
RNAscope probe: Hs-SNTN-C3	ACD	Cat#891411-C3
RNAscope probe: Hs-ZIC1-C2	ACD	Cat#542991-C2
RNAscope probe: Hs-ARX	ACD	Cat#486711
RNAscope probe: Hs-FOXA2-C3	ACD	Cat#832221-C3
RNAscope probe: Hs-PAX6-O1-C3	ACD	Cat#888441-C3
Mm-Ucma-O1-C2	ACD	Cat#468431-C2
RNAscope probe: Hs-PPIB	ACD	Cat#313901
Opal 520	Akoya Biosciences	Cat#FP1487001KT
Opal 570	Akoya Biosciences	Cat#FP1488001KT
Opal 690	Akoya Biosciences	Cat#FP1497001KT
Deposited data		
scRNA-seq (spinal cord ependymal cells, Smart-seq2)	This paper	ArrayExpress: E-MTAB-11563
scRNA-seq (cells from the central canal region of young and aged mice, 10x Genomics)	This paper	ArrayExpress: E-MTAB-11561
Code for scRNA-seq data analysis	This paper	GitHub: https://github.com/aidarodrigo/ependymal_cell; Zenodo: https://doi.org/10.5281/zenodo.7459071
Experimental models: Organisms/strains		
Mouse: *B6;C3-Tg(FOXJ1-EGFP)85Leo/J*	Ostrowski et al.[46]	RRID:IMSR_JAX:010827
Mouse: Foxj1-CreER^{T2} B6;129S6-Gt(ROSA)26Sor$^{tm9(CAG-tdTomato)Hze}$/J	Meletis et al.[11] RRID:IMRS_JAX:007905	N/A
Mouse: C57BL/6J	Charles River	RRID:IMSR_JAX:000664
Mouse: aged C57BL/6J	Charles River	RRID:IMSR_JAX:000664
Software and algorithms		
Fiji	Schindelin et al.[91]	https://imagej.net/software/fiji/
Cell Ranger v4.0	10x Genomics	https://support.10xgenomics.com/single-cell-gene-expression/software/overview/welcome
cutadapt v1.16	Martin[92]	https://cutadapt.readthedocs.io/en/stable/
clustree v.0.4.3	Zappia and Oshlack[93]	https://cran.r-project.org/web/packages/clustree/
Seurat v3.2.2	Stuart et al.[94]	https://satijalab.org/seurat/
STAR 2.7.7a	Kaminow et al.[95]	https://github.com/alexdobin/STAR
g:Profiler	Raudvere et al.[96]	https://biit.cs.ut.ee/gprofiler/gost

(*Continued on next page*)

Continued

REAGENT or RESOURCE	SOURCE	IDENTIFIER
bamtofastq v1.2.0	10x Genomics	https://github.com/10XGenomics/bamtofastq/releases
loomR	Stuart et al.[94]	https://github.com/mojaveazure/loomR
ggplot2	Wickham[97]	https://ggplot2.tidyverse.org/
BD FACSDiva Software	BD Bioscience	https://www.bdbiosciences.com/en-gb/products/software/instrument-software/bd-facsdiva-software
TapeStation Analysis Software	Agilent Technologies, Inc.	https://www.agilent.com/en/product/automated-electrophoresis/tapestation-systems/tapestation-software/tapestation-software-379381
Leica LAS X	Leica Microsystems	https://www.leica-microsystems.com/products/microscope-software/p/leica-las-x-ls/
Adobe Illustrator CS6	Adobe	https://www.adobe.com/products/illustrator.html
Adobe Photoshop CS6	N/A	https://www.adobe.com/products/photoshop.html
Other		
Accession numbers of scRNA-seq data from Zeisel et al.[38] used in this study	Zeisel et al.[38]	Table S7
BD Influx Cell Sorter	BD Biosciences	N/A
Leica VT1200 semi-automatic vibrating blade microtome	Leica Biosystems	https://www.leicabiosystems.com/en-gb/research/vibratomes/leica-vt1200/
NovaSeq 6000	Illumina	https://emea.illumina.com/systems/sequencing-platforms/novaseq.html
TCS SP8 confocal laser scanning microscope system	Leica	N/A
TapeStation	Agilent Technologies, Inc.	N/A

RESOURCE AVAILABILITY

Lead contact

Further information and requests for resources and reagents should be directed to and will be fulfilled by the lead contact, Kate G. Storey (k.g.storey@dundee.ac.uk).

Materials availability

This study did not generate new unique reagents.

Data and code availability

- Raw scRNA-seq data, count matrices, and metadata of all the datasets generated in this paper have been deposited at ArrayExpress under accession numbers ArrayExpress: E-MTAB-11561 (10x Genomics) and ArrayExpress: E-MTAB-11563 (Smart-seq2). This paper also analyses publicly available data from Zeisel et al.[38] These accession numbers are listed in the key resources table. The human developing spinal cord microscopy data can be found at: https://hdbratlas.org/organ-systems/nervous-system/cns/spinal-cord/CS13-18-rnascope.html . Other microscopy data reported in this paper will be shared by the lead contact upon request.
- The code used for scRNA-seq data analysis can be found at GitHub: https://github.com/aidarodrigo/ependymal_cell and Zenodo: https://doi.org/10.5281/zenodo.7459071
- Any additional information required to reanalyze the data reported in this paper is available from the lead contact upon request.

EXPERIMENTAL MODEL AND SUBJECT DETAILS

Animals

FOXJ1-EGFP transgenic mice[46] were used for the generation of the Smart-seq2 scRNA-seq dataset (2.5 to 3-month-old) and for RNAscope experiments (E18.5, P21, and 3-month-old). For timed matings, the morning of the plug was considered E0.5. C57BL/

6J wild-type mice (Charles River) were used for the generation of 10x scRNA-seq datasets (3 to 4 and 18 to 19-month-old mice), for RNAscope (18-month-old mice) and spinal cord slice culture experiments (5-month-old mice). All mice used in scRNA-seq experiments were females, while female and male mice were used for RNAscope and slice culture experiments. Animals were housed in standard housing conditions on a 14-hour light/10-hour dark cycle with food and water ad libitum. All animal procedures for scRNA-seq, RNAscope, and spinal cord slice culture experiments were performed in accordance with UK and EU legislation and guidance on animal use in bioscience research. This work was performed under the UK project license 60/4454 and P0B7F2E8D and subjected to local ethical review.

For spinal cord injury experiments, Foxj1-CreER^{T2} mice[11] were crossed with tdTomato Cre reporter mice[98] (JAX stock number 007905) to generate Foxj1-CreER^{T2}-LSL-tdTomato mice. 6 to 7-month-old Foxj1-CreERT2-LSL-tdTomato mice were used for experiments. Animals were housed in the Wallenberg Laboratory animal facility on a 12-hour light/dark cycle and were provided food and water ad libitum. Spinal cord injury experiments were performed in accordance with the Swedish and European Union guidelines and approved by the institutional ethical committee (*Stockholms Norra Djurförsöksetiska Nämnd*) under ethical permit 20785/2020.

Human samples

Human spinal cord samples were obtained from The Netherlands Brain Bank (NBB), Netherlands Institute for Neuroscience, Amsterdam (https://www.brainbank.nl/). All material has been collected from donors for or from whom a written informed consent for a brain autopsy and the use of the material and clinical information for research purposes had been obtained by the NBB. An overview of the clinical information and post-mortem variables of donors in this study can be found in Table S6. Human embryonic tissue (CS18) was obtained from the MRC/Wellcome Trust (grant no. 006237/1) funded Human Developmental Biology Resource (HDBR; www.hdbr.org) with appropriate maternal written consent and approval from the London Fulham Research Ethics Committee (18/LO/0822) and the Newcastle and North Tyneside NHS Health Authority Joint Ethics Committee (08/H0906/21+5). HDBR is regulated by the UK Human Tissue Authority (HTA; www.hta.gov.uk) and operates in accordance with the relevant HTA codes of practice. This work was part of project no. 200407 registered with the HDBR.

METHOD DETAILS

Cell preparation for scRNA-seq

Cell preparation for plate-based scRNA-seq (Smart-seq2)

For the plate-based scRNA-seq dataset, we generated cell preparations from FOXJ1-EGFP mice. A total of four cell preparations were generated, one per day and starting at 10 AM. In parallel to the FOXJ1-EGFP cell preparation we generated a cell preparation from C57BL/6J wild-type mice to set the GFP threshold for sorting. Mice were deeply anaesthetised with an intraperitoneal injection of pentobarbital before being transcardially perfused with ice-cold artificial cerebrospinal fluid (aCSF) solution (87 mM NaCl, 2.5 mM KCl, 1.25 mM NaH_2PO_4, 26 mM $NaHCO_3$, 25 mM glucose, 1 mM $CaCl_2$, 2 mM $MgSO_4$, 10 mM HEPES in sterile MilliQ water, pH 7.4) that was oxygenated in 95% O_2 5% CO_2 until used. After laminectomy, the spinal cord was carefully dissected out and transferred to a Sylgard-coated dish filled with ice-cold aCSF for microdissection. The thoracic region of the spinal cord was separated with a scalpel and pinned, ventral side down, then cut through the midline in two halves as in an open-book preparation. Working under a fluorescence stereo microscope, the central canal of the spinal cord was identified as an opaque stripe running along the middle of either of the halves of the spinal cord or, aided by fluorescence, as a bright GFP stripe. The central canal was quickly microdissected, cut in small pieces, and placed in aCSF on ice until the whole thoracic central canal was microdissected. Quickly, the aCSF was replaced with 1 mL of pre-warmed digestion solution (3X TrypLE Select enzyme (Thermo Fisher Scientific, cat# A1217702) diluted in Hanks' Balanced Salt Solution (HBSS) (Thermo Fisher Scientific, cat# 14025050) without calcium and magnesium, 15 mM HEPES, and 10 μg/ml DNase I (Worthington)) and the tissue pieces incubated in a water bath at 37 °C. After 45 min, tissue pieces were gently pipetted up and down 10x to facilitate their dissociation and immediately returned to the water bath. After 20 min, the remaining tissue pieces and cells were gently pipetted up and down 12x with a P1000 pipette tip and 22x with a P200 pipette tip. The enzymatic digestion was then stopped with wash solution (HBSS, 15 mM HEPES, 0.05% BSA, 0.5 mM EDTA) and the cell suspension filtered through a 50 μm cell strainer (CellTrics, Sysmex Europe) and centrifuged at 300 xg for 5 min. After discarding the supernatant, myelin debris was removed from the cell suspension using Myelin Removal Beads II kit (Miltenyi Biotec, cat# 130-096-731) following the manufacturer's protocol with minor modifications. Briefly, the cell suspension was incubated with the adequate volume of Myelin Removal Beads II for 15 min in the fridge (4 °C), then washed well by adding 10x the beads volume of MACS buffer and centrifuged at 300 xg for 5 min. LS columns with a 30 μm pre-separation filter (Miltenyi Biotec) were equilibrated with MACS buffer on a QuadroMACS magnetic separator (Miltenyi Biotec) and as soon as the cell suspension finished centrifugating, cells were passed through the filter and column to remove cell clumps and myelin debris. The cell suspension was then centrifuged at 300 xg for 5 min and the MACS buffer quickly replaced with sorting buffer (HBSS, 15 mM HEPES, 0.5% BSA, 1 mM EDTA, 5 μg/mL 4,6-diamidino-2-phenylindole (DAPI)) and the cell pellet gently resuspended and placed on ice until cells were sorted into lysis buffer plates. Lysis plates were created by dispensing 0.4 μl lysis buffer (0.5 U Recombinant RNase Inhibitor (Takara Bio, 2313B), 0.0625% Triton X-100 (Sigma, 93443-100ML), 3.125 mM dNTP mix (Thermo Fisher Scientific, R0193), 3.125 μM Oligo-dT 30 VN (IDT, 5'AAGCAGTGGTATCAACGCAGAGTACT 30 VN-3') and 1:600,000 ERCC RNA spike-in mix (Thermo Fisher Scientific, 4456740)) into 384-well hard-shell PCR plates (Biorad HSP3901) using a Tempest liquid handler (Formulatrix). All plates were then spun down for 1 min at 3220 xg and snap frozen on dry ice. Plates were stored at -80°C until used for sorting.

Please cite this article in press as: Rodrigo Albors et al., An ependymal cell census identifies heterogeneous and ongoing cell maturation in the adult mouse spinal cord that changes dynamically on injury, Developmental Cell (2023), https://doi.org/10.1016/j.devcel.2023.01.003

GFP-positive DAPI-negative cells were sorted into lysis plates with a BD Influx Cell Sorter using 6 psi pressure and a 130 μm nozzle. Flow cytometry data was analyzed using BD FACS software. Sorted plates were immediately spun down for 1 min and snap frozen on dry ice until processed.

To maximise cell recovery, wide-mouth low-retention tips pipette tips were used through the cell preparation. Low retention microcentrifuge/Eppendorf tubes were also used throughout. All working solutions were adjusted to pH 7.4. and kept on ice, except the digestion solution that was kept at 37 °C. Spinal cord tissue and cells were kept on ice at all times except during enzymatic digestion.

Cell preparation for droplet-based scRNA-seq (10x Genomics)

For the droplet-based scRNA-seq datasets, we generated samples from 4 young (3 to 4-month-old) and 4 aged (18 to 19-month-old) C57BL/6J mice, with two animals killed per day: one young and one old. To avoid introducing technical bias,[99] the two cell preparations were processed in parallel, alternating which sample was processed first (alternating between 3 to 4-month old sample followed by the 18 to 19-month old sample, and then the 18 to 19-month sample followed by the 3 to 4-month sample). The cell preparation for 10x scRNA-seq was based on that for plate-based scRNA-seq, with some modifications to improve the cell yield and minimise cell clumps: (1) all the solutions used for cell preparations for 10x scRNA-seq contained 1% (w/v) trehalose as we found that it greatly improved cell survival[100] and thus cell yield, (2) we added 50 μg/mL (0.28 collagenase Wünsch units) of Liberase TM (Merck, cat# 5401119001) in the digestion solution, and (3) added an additional digestion step after the myelin removal step. We also added a step to lyse red blood cells with the goal of maximising ependymal cell capture. Briefly, mice were deeply anaesthetised and perfused transcardially with ice-cold, oxygenated aCSF. The spinal cords were carefully dissected out and transferred onto a dish filled with ice-cold aCSF for microdissection. For 10x scRNA-seq cell preparations the whole spinal cord was used, and the central canal was identified as an opaque stripe running along the middle of the spinal cord in an open-book preparation. Microdissected central canal tissue pieces were kept in aCSF on ice until the whole or most of the spinal cord central canal was microdissected for both samples. Tissue pieces were then incubated in pre-warmed digestion solution (3X TrypLE Select enzyme and 50 μg/mL Liberase TM diluted in HBSS without calcium and magnesium, 15 mM HEPES, and 10 μg/ml DNase I, 1% (w/v) trehalose) and incubated in an incubator shaker at 37 °C. Every 15 min, tissue pieces were gently pipetted up and down 10x to facilitate their dissociation. After 65 min of digestion, cell preparations were gently pipetted up and down 12x with a P1000 pipette tip and 22x with a P200 pipette tip and wash solution (HBSS without calcium and magnesium, 15 mM HEPES, 0.4% BSA, 0.1% trehalose) was added to stop the digestions. Cell suspensions were then filtered through a 50 μm cell strainer (CellTrics, Sysmex Europe) and centrifuged at 300 xg for 6 min at 4 °C. Cell pellets were resuspended in red blood cell lysis buffer (Roche, cat# 11814389001) and incubated for 1 min at RT. MACS buffer was then added and cell suspensions centrifuged at 300 xg for 6 min. Myelin debris was removed from the cell suspensions using Myelin Removal Beads II kit (Miltenyi Biotec) as described above but with 1 min longer centrifugation steps. Note that this step seems to deplete most neurons from the cell preparation and thus neurons are underrepresented in 10x datasets. It is also likely that neurons do not survive well our dissociation protocol. Following myelin removal, cell suspensions were incubated in post-digestion solution (3X TrypLE Select enzyme, HBSS without calcium and magnesium, 15mM HEPES, 1 mM EDTA, 1% (w/v) trehalose) for 8 min in the 37 °C incubator shaker. The digestions were stopped with wash solution without EDTA and immediately centrifuged at 300 xg for 4 min. Cell pellets were quickly but gently resuspended in wash buffer without EDTA and kept on ice until loaded into the Chromium controller (10x Genomics). A small aliquot of each cell suspension was mixed with the same volume of Trypan Blue Solution (0.4%) (Thermo Fisher Scientific, cat# 15250061) to estimate cell concentration and cell viability before loading the cell preparations into the Chromium chip (10x Genomics).

Single-cell library preparation and sequencing

Plate-based scRNA-seq

cDNA synthesis was performed using the Smart-seq2 protocol.[101,102] Briefly, 384-well plates containing single-cell lysates were thawed on ice followed by first strand synthesis. 0.6 μl of reaction mix (16.7 U/μl SMARTScribe TM Reverse Transcriptase (Takara Bio, 639538), 1.67 U/μl Recombinant RNase Inhibitor (Takara Bio, 2313B), 1.67X First-Strand Buffer (Takara Bio, 639538), 1.67 μM TSO (Exiqon, 5'-AAGCAGTGGTATCAACGCAGACTACATrGrG+G-3'), 8.33 mM DTT (Bioworld, 40420001-1), 1.67 M Betaine (Sigma, B0300-5VL), and 10 mM MgCl 2 (Sigma, M1028-10X1ML)) was added to each well using a Tempest liquid handler. Bulk wells received twice the amount of RT mix (1.2 μl). Reverse transcription was carried out by incubating wells on a ProFlex 2x384 thermal-cycler (Thermo Fisher Scientific) at 42°C for 90 min and stopped by heating at 70°C for 5 min. Subsequently, 1.6 μl of PCR mix (1.67X KAPA HiFi HotStart ReadyMix (Kapa Biosystems, KK2602), 0.17 μM IS PCR primer (IDT, 5'-AAGCAGTGGTATCAACGCAGAGT-3'), and 0.038U/μl Lambda Exonuclease (NEB, M0262L)) was added to each well with a Tempest liquid handler (Formulatrix). The amplified product was diluted with a ratio of 1 part cDNA to 10 parts 10mM Tris-HCl (Thermo Fisher Scientific, 15568025), and concentrations were measured with dye-fluorescence assay (Quant-iT dsDNA High Sensitivity kit; Thermo Fisher Scientific, Q33120) on a SpectraMax i3x microplate reader (Molecular Devices). These wells were reformatted to a new 384-well plate at a concentration of 0.3 ng/μl and final volume of 0.4 μl using an Echo 550 acoustic liquid dispenser (Labcyte). If the cell concentration was below 0.3 ng/μl, 0.4 μl of sample was transferred.

Illumina sequencing libraries were prepared using the Nextera XT Library Sample Preparation kit (Illumina, FC-131-1096).[92,103] Each well was mixed with 0.8 μl Nextera tagmentation DNA buffer (Illumina) and 0.4 μl Tn5 enzyme (Illumina), then tagmented at 55°C for 10 min. The reaction was stopped by adding 0.4 μl Neutralize Tagment Buffer (Illumina) and spinning at room temperature (RT) in a centrifuge at 3220 xg for 5 min. Indexing PCR reactions were performed by adding 0.4 μl of 5 μM i5 indexing primer, 0.4 μl of 5 μM i7 indexing primer, and 1.2 μl of Nextera NPM mix (Illumina). PCR amplification was carried out on a ProFlex 2x384 thermal

Please cite this article in press as: Rodrigo Albors et al., An ependymal cell census identifies heterogeneous and ongoing cell maturation in the adult mouse spinal cord that changes dynamically on injury, Developmental Cell (2023), https://doi.org/10.1016/j.devcel.2023.01.003

cycler using the following program: 1. 72°C for 3 min, 2. 95°C for 30 s, 3. 12 cycles of 95°C for 10 s, 55°C for 30 s, and 72°C for 1 min, and 4. 72°C for 5 min.

Following library preparation, wells of each library plate were pooled using a Mosquito liquid handler (TTP Labtech). Pooling was followed by two purifications using 0.7x AMPure beads (Fisher, A63881). Library quality was assessed using capillary electrophoresis on a Fragment Analyzer (AATI), and libraries were quantified by qPCR (Kapa Biosystems, KK4923) on a CFX96 Touch Real-Time PCR Detection System (Biorad). Plate pools were normalized to 2 nM and sequenced on the NovaSeq 6000 Sequencing System (Illumina) using 2x100bp paired-end reads with an S4 300 cycle kit (Illumina, 20012866).

Droplet-based scRNA-seq (10x Genomics)

cDNA libraries were generated with 10x Genomics Chromium Single Cell 3' Library and Gel Bead Kit v3.1 following the manufacturer's instructions. Quality control of the cDNA and sequencing libraries was performed using a TapeStation System (Agilent) with High Sensitivity D5000 ScreenTape and library concentrations were measured with Qubit dsDNA High Sensitivity assay kit (Thermo Fisher Scientific, cat# Q32851). The eight libraries (one for each mouse) were then pooled for sequencing, taking into account the expected differences in cell numbers between each library. Sequencing was performed by Edinburgh Genomics (University of Edinburgh) on two lanes of a NovaSeq 6000 Sequencing System (Illumina) with the following cycle setup for paired-end reads: read 1, 28 cycles; i7 index, 8 cycles; read 2, 91 cycles).

scRNA-seq data preprocessing

Plate-based scRNA-seq (Smart-seq2)

Raw sequencing reads were trimmed to remove contaminating adapter sequences and low-quality ends (using a cutoff threshold of 15) with cutadapt v1.16.[104] Reads shorter than 75 nucleotides were filtered out. Trimmed and paired reads were then aligned to the mouse reference genome (mm10, Ensembl release 98) enhanced with ERCC spike-in and EGFP sequences and quantified using the STARsolo pipeline within STAR 2.7.7a.[95,105] The output of STARsolo is similar to that of Cell Ranger,[95] which we used to generate the count matrices from the 10x data. STAR parameters were: –soloType SmartSeq –soloUMIdedup Exact –soloStrand Unstranded –sjdbOverhang 99 –outFilterType BySJout –outFilterMultimapNmax 20 –outSAMtype BAM SortedByCoordinate –outSAMattributes All –outSAMunmapped Within KeepPairs –quantMode GeneCounts TranscriptomeSAM. Remaining parameters were set to default values. Gene count matrices were then loaded into Seurat v3.2.2[94] for further analysis.

Droplet-based scRNA-seq (10x)

Raw sequencing reads were preprocessed with Cell Ranger v4.0 (10x Genomics) following the manufacturer's instructions with default parameters and aligned to the mouse reference genome (mm10, Ensembl release 100). The output filtered feature-barcoded matrices (count matrices) were then loaded into Seurat v3.2.2[94] for further analysis.

scRNA-seq quality control, normalization, and dimensionality reduction

All gene count matrices were merged by dataset and processed using Seurat v3.2.2.[94] Cells expressing fewer than 500 genes and genes expressed in fewer than 3 cells were removed. Smart-seq2 data were normalized with a scale factor of 1,000,000 and 10x data were normalized with a scale factor 10,000 then log transformed using Seurat's NormalizeData function. Highly variable features were identified with the FindVariableFeatures function using the vst method with default parameters. After scaling and centring the data, the top 2,500 highly variable features were used for principal component analysis (PCA) and significant principal components (PCs) were used for graph-based clustering (shared nearest neighbour graph and Louvain clustering using Seurat's FindClusters function). The same PCs were used as input to uniform manifold approximation and projection (UMAP)[106] for data visualization. Clustering was performed at a range of clustering resolutions and the R package clustree v0.4.3[93] was used to visualize and understand relationships between clusters, in combination with differential expression analyses. The most biologically meaningful clustering resolution was chosen. To annotate cell clusters, differential expression analyses were performed using a Wilcoxon rank sum test. Cell clusters were manually annotated based on known marker genes and data from www.mousebrain.org.[38] Clusters that co-expressed mutually exclusive markers (i.e. markers that define distinct cell types) were considered doublets and removed from the datasets. A few, small non-ependymal cell clusters (e.g. microglia) were removed from the Smartseq2 dataset. After removing potential doublets and contaminating cells, highly variable features, PCA, clustering and visualization was repeated as described above until no more doublets or contaminating cells remained in the datasets. The resulting datasets were aggregated or integrated as described below.

Ependymal cell heterogeneity analysis

After initial quality control, filtering, and annotating the 10x dataset of cells from the spinal cord central canal region of young adult mice, we subset the ependymal cell cluster to integrate it with the Smart-seq2 ependymal cell dataset using Seurat's canonical correlation analysis (CCA).[94] After finding integration anchors and running the IntegrateData function, the workflow described above for PCA, clustering, and data visualization was performed on the integrated dataset to explore ependymal cell heterogeneity. Multiple rounds of differential expression testing were performed on the raw (non-integrated) normalised counts using the functions FindAllMarkers, to identify markers of a cluster compared to all the other cells, and FindMarkers, to identify markers genes that differentiate two specific clusters. A Wilcoxon rank sum test was used for all differential expression testing with a log-fold change threshold of 0.25 and on genes detected in a minimum of 15% of the cells in each cluster. Cell identities were assign based on known markers and informed by marker genes and our own findings for mature lateral cells. Clusters that were not defined by the expression of

Please cite this article in press as: Rodrigo Albors et al., An ependymal cell census identifies heterogeneous and ongoing cell maturation in the adult mouse spinal cord that changes dynamically on injury, Developmental Cell (2023), https://doi.org/10.1016/j.devcel.2023.01.003

unique markers were merged with the closest cluster based on pair-wise differential expression analysis and guided by clustering tree visualizations. A phylogenetic tree relating the average cell from each cluster (Figure 2B) was estimated based on a distance matrix constructed in the integrated counts space using Seurat's BuildClusterTree function.

Ependymal cell ageing analysis

Filtered 10x datasets from cells in the spinal cord central canal region of young adult and aged mice were aggregated and processed using Seurat v3.2.2.[94] An initial analysis was performed as described in "scRNA-seq quality control, normalization, and dimensionality reduction" to take advantage of the larger number of cells in the aggregated dataset in identifying cell clusters and marker genes. We then subset the ependymal cell cluster to study ependymal cell heterogeneity and age-related changes in gene expression and cellular composition. Highly variable features were identified with Seurat's FindVariableFeatures function using the vst method with default parameters. The top 2,500 highly variable features were used for PCA and significant PCs were used for graph-based clustering (shared nearest neighbour graph and Louvain clustering). The same PCs were used as input to UMAP. Clustering was performed at a range of resolutions and clustree was used to visualise relationships between clusters and to identify the most biologically meaningful clustering resolution. After performing differential expression testing using a Wilcoxon rank sum test, cell identities were assigned to each cluster based on known marker genes and data from www.mousebrain.org.[38] A cell cluster characterised by the co-expression of markers of astrocytes and ependymal cells was removed after we could not confirm the existence of such cells in the tissue. A 3-cell cluster that expressed choroid plexus genes was also removed from the dataset. After removing potential doublets and contaminating cells, highly variable features, PCA, clustering and visualization was repeated as described above. Multiple rounds of differential expression testing were performed using the functions FindAllMarkers and FindMarkers. A Wilcoxon rank sum test was used for all differential expression testing with a log-fold change threshold of 0.25 and on genes detected in a minimum of 15% of the cells in each cluster. Cell identities were assign as described in our ependymal cell heterogeneity analysis and clusters that were not defined by the expression of unique markers were similarly merged with the closest cluster based on pair-wise differential expression analysis and guided by clustree. Differential expression analysis was performed to identify age-related changes in gene expression in the ependymal cell population. To do so, age (young or aged) was assigned as cell identities and Seurat's FindMarkers function with a log-fold change threshold of 0.2 was used to identify genes that were up- or downregulated in cells from aged mice in at least 25% of the cells. To calculate the fraction of each ependymal cluster in each sample, the number of cells from each sample in a given cluster was calculated and normalised to the number of cells per sample. A two-sided Wilcoxon rank sum test was then performed to test for significant differences in the fractions of cluster between young and aged mice using base R. P-values below 0.05 are indicated in Figure 3D.

Ependymal cells across the CNS analysis

scRNA-seq data of ependymal cells from across the CNS were obtained from Zeisel et al.[38] First, we downloaded a loom file including curated ependymal cell transcriptomes from www.mousebrain.org (l6_r4_ependymal_cells.loom). This file was read with Seurat via loomR to extract from which 10x runs these cells were captured and then the raw sequencing reads downloaded for preprocessing and integration with our 10x dataset. All relevant BAM files were converted to FASTQ files using bamtofastq v1.2.0 (10x Genomics) and preprocessed using the same workflow as described above for our 10x data (see "scRNA-seq data preprocessing droplet-based scRA-seq"). Count matrices were loaded to Seurat for further analysis. Data from the following tissues were included: amygdala, hypothalamus, hippocampus, striatum, midbrain, thalamus, pons, medulla, and spinal cord. After removing cells expressing fewer than 500 features and genes detected in fewer than 3 cells, the filtered data were normalized with a scale factor of 10,000 UMIs per cell and then log transformed. Highly variable features were identified with Seurat's FindVariableFeatures function using the vst method with default parameters. The top 2,200 highly variable features were used for PCA and significant PCs were used for graph-based clustering (shared nearest neighbour graph and Louvain clustering using Seurat's FindClusters function). The same significant PCs were used as input to UMAP. Clustering was performed at a range of resolutions and clustree was used to visualize relationships between clusters and this, in combination with differential expression analyses, was used to set the most biologically meaningful clustering resolution. Informed by differentially expressed genes, cell clusters were annotated based on known marker genes and data from www.mousebrain.org. Clusters assigned to ependymal cells were subset from the dataset and the workflow repeated, from the identification of highly variable genes step to differential expression testing between clusters. Clusters of non-ependymal identity were removed and the workflow repeated again until the dataset contained only ependymal cells. Next, we integrated the Zeisel dataset with our 10x spinal cord ependymal cell dataset from young adult mice using Seurat's CCA.[94] To minimise technical artefacts and challenges due to different Chromium Single Cell 3′ chemistries used to generate the 10x datasets, we kept only genes that were detected in both datasets. The data were merged, normalised with a scale factor of 10,000 UMIs per cell and then log transformed. Highly variable features were identified with Seurat's FindVariableFeatures function and the vst method. After selecting 2,000 integration features with the function SelectIntegrationFeatures, finding integration anchors and running the IntegrateData function, the standard workflow for PCA, clustering, and data visualisation was performed on the integrated counts. Multiple rounds of differential expression testing were performed on the raw (non-integrated) normalised counts. A Wilcoxon rank sum test was used for all differential expression testing with a log-fold change threshold of 0.25 and on genes detected in a minimum of 25% of the cells in each cluster. Following this, a microglia cluster and a cluster of potential astrocyte and ependymal cell doublets were removed from the dataset and the workflow described above ran again from finding integration anchors and integrating the data, to performing PCA and selecting significant PCs, clustering at a range of resolutions, visualizing the data with UMAP,

and performing differential expression testing to assign cell identities. Cell identities were assign based on known markers and the tissue of origin as recorded in each cell's metadata. Clusters not defined by the expression of unique markers were merged with the closest cluster based on pair-wise differential expression analysis and their relationship with other clusters as visualised with clustree.

Data visualization

UMAP plots showing gene expression patterns were generated using the R package ggplot2[97] and the viridis colour palette.[107] Stacked bar plots, bar plots, and boxplots were also generated with ggplot2. All other plots were generated with Seurat v3.2.2.

GO enrichment analysis

Marker gene lists were generated using Seurat's FindAllMarkers or FindMarkers functions and based on the non-parametric Wilcoxon rank sum test with Bonferroni correction. Genes with an adjusted p-value below 0.05 were considered to be differentially expressed. Marker gene lists for each cluster were uploaded as input to g:Profiler for functional profiling (https://biit.cs.ut.ee/gprofiler/gost).[96] Marker genes lists were ordered from the most significant to the least significant adjusted p-value. GO enrichment analysis was performed using the hypergeometric test and Benjamini-Hochberg FDR correction for multiple testing. GO terms, KEGG, Reactome or WikiPathways with an adjusted p-value below 0.01 were reported.

Dual RNAscope and immunofluorescence

Mouse samples

Mice aged 21 days (P21), 3 months and 18 months were anaesthetised and then perfused transcardially with ice-cold phosphate buffered saline (PBS). The spinal cord was quickly dissected and fixed in ice-cold 4% paraformaldehyde (PFA) for 2 h at 4 °C (RT). E18.5 embryos were dissected in ice-cold PBS and their spinal cord fixed in ice-cold 4% PFA for 2 h at 4 °C. Spinal cord slices from spinal cord slice culture experiments were fixed in ice-cold 4% PFA for 2 h at 4 °C. After fixing, all samples were washed in PBS and equilibrated in 30% sucrose/PBS overnight at 4°C before embedding in OCT (Sakura Tissue-Tek) and storing at -80 °C until processed. Samples were cryosectioned in 10 μm-thick sections and collected in Superfrost Plus slides (Fisher Scientific). RNAscope was performed following the manufacturer's RNAscope Multiplex Fluorescent Reagent Kit v2 Assay manual (Advanced Cell Diagnostics). Briefly, sections were thawed then covered in Hydrogen Peroxidase for 10 min at RT, washed twice with distilled water, incubated with RNAscope Protease IV for 5 min at RT then washed immediately with PBS. Probes were hybridized for 2 h at 40 °C in RNAscope's HybEZ oven then amplified. After washing the slides, we proceeded directly to perform immunofluorescence for GFP. Slides were washed twice 2 min with PBS containing 0.1% Triton X-100 (PBST), blocked for 1 h in blocking buffer (PBST with 10% donkey serum) and incubated with the primary antibody chicken anti-GFP (1:250 in blocking buffer) (Abcam, ab13970) overnight at 4 °C. Slides were washed 3x 5 min in PBST and then incubated with secondary antibody overnight at 4 °C. The following day, slides were washed 3x 5min in PBST, counterstained with DAPI and mounted with SlowFade™ Gold Antifade Mountant (Thermo Fisher Scientific).

RNAscope probes used were: Mm-Sntn-C3 (ACD cat# 574191-C3), Mm-Vtn-C3 (ACD cat# 443601-C3), Mm-Zic1 (ACD cat# 493121), Mm-Wnt4-C2 (ACD cat# 401101-C2), Mm-Dkk3 (ACD cat# 400931), Mm-Mia (ACD cat# 400911), Mm-Fos (cat# 316921), Mm-Bhmt (cat# 876991), Mm-Ucma-O1-C2 (cat# 468431-C2). Opal™ dyes used were: Opal 520 (cat# FP1487001KT), Opal 570 (cat# FP1488001KT), and Opal 690 (cat# FP1497001KT) (Akoya Biosciences).

Human samples

Fresh-frozen human spinal cord samples (Table S6) from the NBB were serially cryosectioned in 10 μm-thick sections and collected in Superfrost Plus slides. Human embryonic tissue from the HDBR was fixed in 4% PFA for 2 h at 4°C then washed in PBS and cryoprotected in 30% sucrose overnight, embedded and frozen for cryosectioning, RNAscope was carried out following the manufacturer's RNAscope Multiplex Fluorescent Reagent Kit v2 Assay manual for fresh frozen tissue (Advanced Cell Diagnostics). Briefly, sections were fixed 15 min with fresh, ice-cold 4% PFA and then rinsed 2 times with PBS. Sections were then dehydrated in a series of steps with solutions of increasing ethanol concentration in PBS and then covered with RNAscope Hydrogen Peroxidase for 10 min at RT and washed twice with distilled water. Sections were incubated with RNAscope Protease IV for 2 min at RT then washed immediately with PBS. Probes were hybridized for 2 h at 40 °C in RNAscope's HybEZ oven and then amplified. After washing the slides, we proceeded directly to perform immunofluorescence for FOXJ1. Slides were washed twice 2 min with PBST, blocked for 1 h in blocking buffer, and incubated with primary antibody rabbit anti-FOXJ1 (1:50 in blocking buffer) (Sigma-Aldrich, HPA005714) overnight at 4 °C. Slides were washed 3x 5 min in PBST and then incubated with secondary antibody overnight at 4 °C. The following day, slides were washed 3x 5min in PBST, counterstained with DAPI and mounted with SlowFade™ Gold Antifade Mountant. RNAscope probes used were: Hs-SNTN (ACD cat# 891411), Hs-ZIC1 (ACD cat# 542991), Hs-ARX (ACD cat# 486711), Hs-PPIB (ACD cat# 313901), Hs-FOXA2-C3 (ACD, cat# 832221-C3), Hs-PAX6-O1-C3 (ACD, cat# 888441-C3). Opal™ dyes used were: Opal 570 (cat# FP1488001KT), and Opal 690 (cat# FP1497001KT).

Spinal cord slice culture

Spinal cord slice culture experiments were carried out following Fernandez-Zafra et al.[80] with some modifications. Briefly, 5-month-old mice were anaesthetised and then perfused transcardially with ice-cold, oxygenated aCSF and the spinal cord quickly dissected out in ice-cold aCSF. The thoracic region of the spinal cord was then quickly embedded in 4% low-melting point agarose in PBS

Please cite this article in press as: Rodrigo Albors et al., An ependymal cell census identifies heterogeneous and ongoing cell maturation in the adult mouse spinal cord that changes dynamically on injury, Developmental Cell (2023), https://doi.org/10.1016/j.devcel.2023.01.003

(Thermo Fisher Scientific) and 350 μm spinal cord slices were cut in ice-cold oxygenated aCSF using a vibratome (Leica VT1200). 3-4 spinal cord slices from each mouse were fixed in 4% PFA for 2 h at 4°C immediately after vibratome sectioning to serve as the normal condition in our experiments. The rest of spinal cord slices were quickly transferred to 30 mm cell culture inserts (Millipore Sigma) previously coated with 10 mg/mL of poly-L-lysine (Millipore Sigma). Each insert with up to 4 spinal cord slices was then placed in a well of a 6-well plate filled with 1.5 mL of culture medium (50% Neurobasal-A; B-27; 25% heat inactivated horse serum; 25% HBSS; 0.25 mM GlutaMax, 15 mM D-glucose; 15 mM HEPES; and 25 μg/ml penicillin/streptomycin). Every other day, 750 μl of culture medium was replaced with fresh culture medium without disturbing the spinal cord slices or introducing introduce air bubbles. The spinal cord slices were kept in a humidified incubator at 37 °C with a 5% CO_2 atmosphere. At the time of collection, cultured spinal cord slices were fixed in ice-cold 4% PFA for 2 h at 4 °C, then washed in PBS and equilibrated in 30% sucrose/PBS overnight at 4 °C before embedding in OCT and storing at -80 °C until processed. Dual RNAscope and immunofluorescence using probes Mm-Sntn-C3 (ACD cat# 574191-C3) and Mm-Mia (ACD cat# 498011) and rat anti-Ki67 antibody (1:100) (Thermo Fisher Scientific, cat# 14-5698-82; RRID:AB_10854564) was performed as described above for mouse samples.

Spinal cord injury

To induce recombination prior to injury, all Foxj1-CreER^{T2}-LSL-tdTomato mice received 2 mg of tamoxifen intraperitoneally dissolved in 1:9 ethanol:corn oil on two consecutive days. Spinal cord injuries were performed 4 weeks after tamoxifen administration to prevent post-injury recombination. Dorsal funiculus incision injuries were performed as previously described.[20] Briefly, mice were deeply anesthetized with isoflurane and provided with analgesia (Buprenorphine, Schering-Plough, 0.1 mg/kg body weight and Carprofen, Pfizer, 5 mg/kg body weight). After a T8-T9 laminectomy, the dura mater was removed and the dorsal surface of the spinal cord was exposed. After the administration of local anaesthesia (Xylocaine/Lidocaine, AstraZeneca, 10 mg/ml, 2 drops on the spinal cord surface) the dorsal funiculus and adjacent grey matter were cut transversely with microsurgical scissors and the incision was extended rostrally to span one segment. The wounds were sutured, and animals were then returned to their home cage for recovery. Animals were euthanized via intraperitoneal injection of an overdose of sodium pentobarbital. Animals were then transcardially perfused first with D-PBS (Gibco) and then with 4% formaldehyde. Spinal cords were postfixed in 4% formaldehyde overnight at 4°C, washed in D-PBS, equilibrated in 30% sucrose/PBS overnight at 4 °C before embedding in O.C.T. and storing at -80 °C until processed.

Imaging and image processing

All images were acquired with a Leica TCS SP8 confocal laser scanning microscope (Leica Microsystems). All images are shown as maximum intensity projections of acquired z-stacks of about one cell thickness (6-10 μm). Images of the human spinal cord were taken as tiled z-stacks and were stitched together using the stitching algorithm in the Leica Application Suite X (LAS X) software. A minimum of two composite images were taken from each human spinal cord sample and a minimum of 5 images were taken from each mouse. Human spinal cord samples, especially those from older individuals, showed relatively high levels of autofluorescence (probably from lipofuscin granules). The probe against the broadly expressed gene *PPIB* was used to (1) control for RNA quality and (2) to differentiate autofluorescence and unspecific probe binding, identified as overlapping *PPIB* and *SNTN* signal, from real signal. Images from outside of the human ependyma were also acquired to get a sense of the level of unspecific binding of the probes. All images were prepared for publication using Fiji.[91] In some cases, linear parameters (brightness and contrast) needed to be adjusted. These adjustments were always applied equally across the entire image. An additional processing step was required to remove FOXJ1 antibody aggregates (which appear as puncta) in the images in Figures 6C and 6D, added during the paper revision. Aggregates were removed using the function Remove Outliers in Fiji.[91] This step was only applied to the FOXJ1 (grey) channel and not to the RNAscope channels (where the signal appears as puncta).

QUANTIFICATION AND STATISTICAL ANALYSIS

Images were analyzed using Fiji and cells counted with the Cell Counter plugin.[91] For quantification of cells expressing marker genes across ages, ependymal cells were identified based on GFP immunofluorescence and DAPI-stained nuclei in samples from FOXJ1-EGFP spinal cords, and based on location within the central canal walls and nuclear morphology as revealed by DAPI (i.e. small oval nucleus with dense chromatin and multiple nucleoli) in spinal cords from wild-type mice. All ependymal cells within a 10 μm confocal z-stack were counted. Ependymal cells labelled with one or more RNAscope dots either within the GFP-filled cytoplasm in samples from FOXJ1-EGFP mice or within 2-3 μm of the nucleus were considered positive. For quantification of the fractions of *Sntn* and Ki67-positive cells in cultured spinal cord slices and injured spinal cord samples from Foxj1-tdTomato mice, ependymal cells were identified as *Mia*-expressing cells by RNAscope and as tdTomato-labelled cells by immunofluorescence, respectively. All ependymal cells in a single optical slice of a 10 μm z-stack were counted. Ependymal cells with one or more *Sntn* RNAscope within 2-3 μm of the nucleus were considered *Sntn* cells. Ki67-positive cells were identified based on nuclear Ki67 signal. In Foxj1-tdTomato samples, both ependymal cells remaining around the spinal cord central canal and their migrating progeny were labelled. We limited the counts to ependymal cells making up the central canal or with a connexion to it to make the quantification comparable to those in the *ex vivo* assay. Quantification of the fraction of cells expressing a gene in human spinal cord samples was challenging due to tight packing of ependymal cells, differing sample quality, and autofluorescence, especially in tissue from older age groups. We thus report descriptive information about gene expression patterns for these samples.

Please cite this article in press as: Rodrigo Albors et al., An ependymal cell census identifies heterogeneous and ongoing cell maturation in the adult mouse spinal cord that changes dynamically on injury, Developmental Cell (2023), https://doi.org/10.1016/j.devcel.2023.01.003

No statistical method was used beforehand to determine sample size. The investigators were not blinded, and no data points were excluded. Data is represented as mean ± SD. The number of replicates as well as the type of statistical test performed is indicated in each figure legend where relevant.

ADDITIONAL RESOURCES

An interactive web application to further explore the spinal cord ependymal cell census and the ageing dataset is available at: https://ependymalcell.shinyapps.io/ependymal_atlas/.